2022

Synthesis and Characterization of Ruthenium Complexes and Their Potential and Photosensitizers for Photodynamic Therapy

Keit Dine

LOYOLA UNIVERSITY CHICAGO

SYNTHESIS AND CHARACTERIZATION OF RUTHENIUM COMPLEXES AND THEIR POTENTIAL AS PHOTOSENSITIZERS FOR PHOTODYNAMIC THERAPY

A THESIS SUBMITTED TO

THE FACULTY OF THE GRADUATE SCHOOL

IN CANDIDACY FOR THE DEGREE OF

MASTER OF SCIENCE

PROGRAM IN CHEMISTRY AND BIOCHEMISTRY

BY

KEIT DINE

CHICAGO, IL

MAY 2022

ACKNOWLEDGMENTS

I would like to express my sincere appreciation and thanks for the people without whom this work would not have been possible. I want to begin by thanking my incredible advisor, Dr. Wei-Tsung Lee. He challenged and encouraged me to pursue my interests and taught me how to conduct evidence-based research. Your advice, guidance, and support throughout my undergraduate and graduate work has been nothing short of incredible. I want to thank you for everything you have done for me and my fellow lab members.

Next, I want to thank my wonderful committee members, Dr. Daniel P. Becker and Dr. Dali Liu. Additionally, I thank Dr. Matthias Zeller for his crystallography work. I want to thank all the members of Lee lab, both current and former, for their support. Special appreciation goes to Dr. Adri Lugosan, PhD, Bailey Hanson, Winnie Jiang, Erwin Weerawardhana, and the current undergraduate students. I feel honored and privileged to work and learn alongside you and I am excited to see all the amazing things you will accomplish in the future. I want to particularly thank my friends for keeping me grounded with endless hangouts and dinners during my time at Loyola.

Lastly, I would like to thank my parents, Marsela and Astrit Dine. Thank you for your courage in leaving your home country in search for a better life for our family. Your sacrifice continues to inspire me.

Dedicated to my family, friends, and mentors.

TABLE OF CONTENTS

LIST OF TABLES

LIST OF FIGURES

LIST OF SCHEMES

LIST OF ABBREVIATIONS

^{1}LC	Singlet ligand centered
^{1}PS	Singlet ground state
^{1}PS*	Singlet excited state
$^1O_2$	Singlet oxygen
^{3}MLCT	Triplet metal-ligand charge transfer
$^3O_2$	triplet oxygen
^{3}PS*	triplet excited state
6,6,-dmb	6,6’-dimethyl-2,2’-bipyridine
Bpy	2,2’-bipyridine
CDC	Centers for Disease Control and Prevention
Co	Cobalt
Cu_2O	Copper(I) oxide
CV	Cyclic voltammetry
DCM	dichloromethane
DMF	dimethylformamide
Dppz	dipyrido[3,2-a:2’3'-c]phenazine
Fc	Ferrocenium
$FcPF_6$	Ferrocenium hexafluorophosphate
FDA	Food and Drug Administration

Fe	Iron
H_2O_2	Hydrogen peroxide
$HO^{\bullet}$	Hydroxyl radical
t-BuOK	Potassium *tert*-butoxide
LDA	Lithium diisopropylamide
MeCN	Acetonitrile
$MgSO_4$	Magnesium sulfate
N_2	dinitrogen
N_{CZ}	carbazole nitrogen
NH_4Cl	Ammonium chloride
NH_4OH	Ammonium hydroxide
Ni	Nickel
NMR	Nuclear magnetic resonance
N_{Pyr}	Pyrazole nitrogen
O_2	Oxygen
PDT	Photodynamic therapy
Phen	1,10-phenanthroline
PPh_3	Triphenylphosphine
PS	Photosensitizer
Pt	Platinum
ROS	Reactive oxygen species
Ru	Ruthenium
THF	tetrahydrofuran
TMEDA	*N,N,N,N*-tetramethyl-ethylenediamine
UV-vis	UV-visible
Zn	Zinc

ABSTRACT

Cancer is one of the leading causes of death in the world with over 10 million people dying of the disease every year. Inorganic complexes supported by platinum metal centers are often used in cancer treatment. However, these complexes lack selectivity for tumor cells. As such, other alternatives to platinum have been explored. Ruthenium (Ru) complexes are one of the most promising candidates due to their ability to be used as photosensitizing drugs in photodynamic therapy.

Herein, we report the design, synthesis, and characterization of two novel ruthenium-based complexes. One compound is a Ru(II) homoleptic complex, while the other is a mononuclear Ru(II) complex that features an open coordination site. To probe the structural and electronic properties of these complexes, we used nuclear magnetic resonance spectroscopy, X-ray crystallography, UV-visible spectroscopy, and cyclic voltammetry. Future work for this project involves measuring whether our complexes can generate singlet-oxygen in vitro upon irradiation with light.

CHAPTER I

AN INTRODUCTION TO PHOTODYNAMIC THERAPY, RUTHENIUM COMPLEXES, THEIR APPLICATION AS PHOTOSENSITIZERS, AND EXPERIMENTAL DESIGN

Inorganic Complexes Indicated for Cancer

According to the CDC, cancer is one of the leading causes of death in the United States, second only to heart disease. In 2020 alone, nearly 600,000 deaths were attributed to cancer.[1,2] Cancer, which is characterized by unregulated cell growth that can metastasize to other parts of the body, has been the subject of much research. Past work in this field has focused on understanding the biochemical and genetic causes of cancer, how the disease manifests clinically, and developing new therapeutics to treat it. Current cancer treatment protocols involve the use of chemotherapeutics, surgical removal of tumors, and the application of radiation, among other treatment types.[3] Despite the diversity of treatment options, there is an increasing focus to develop more treatments generally, and more novel chemotherapy drugs specifically. In 2020 for instance, nearly half of all the drugs approved by the FDA were indicated for cancer.[4] The need for novel chemotherapies is a consequence of growing drug resistance among many different types of cancer.[5,6] As a result of increasing drug resistance, there is a medical need to develop new anticancer drugs. One growing area of interest is to explore inorganic complexes as novel, small-molecule chemotherapeutics.[7]

An often-overlooked application of transition metal complexes is their use as medicinal agents. Though inorganic complexes have been widely explored for catalysis, small-molecule

activation, and active-site modeling, there is less robust literature supporting their use as drugs compared to their organic counterparts. The lack of interest in considering coordination complexes during the drug discovery process is likely due to the belief that metal-based compounds are inherently dangerous and toxic.[7] However, there are examples of metallodrugs that have both diagnostic and therapeutic applications.[8] For instance, one of the most common metals used in medicine is platinum (Pt). Inorganic compounds supported by Pt are ubiquitous in current cancer treatments. Indeed, about 50% of all cancer treatment regiments incorporate Pt-based anticancer drugs.[9] This statistic demonstrates the potential for inorganic compounds in medicine.

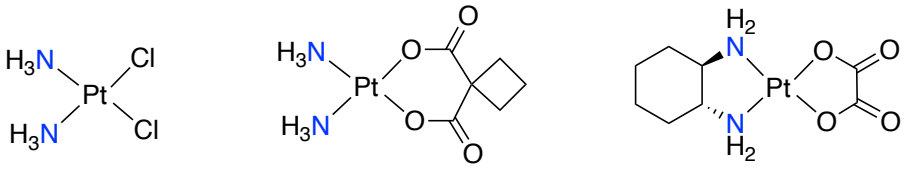

cisplatin **carboplatin** **oxaliplatin**

Figure 1. Platinum-based anticancer drugs. Cisplatin, carboplatin, and oxaliplatin are the three FDA approved medications which are supported by a Pt metal center. The Pt is in the +2 oxidation state and in a square planar geometry for all three compounds.

Platinum-based Chemotherapy Drugs

Thus far, three Pt-based anticancer drugs have been approved by the FDA for clinical use: cisplatin, carboplatin, and oxaliplatin (Figure 1).[10] Of these, cisplatin is one of the most well-known, widely studied, and used coordination compounds in medicine. Cisplatin, or *cis*-$[Pt(NH_3)_2Cl_2]$, is a square-planar coordination complex where two ammine and two chloro ligands are oriented *cis* around a Pt(II) center. Clinically, cisplatin has been used to treat different types of cancer including bladder cancer, ovarian cancer, and testicular cancer.[11–14] However, cisplatin has several serious side effects. The drug has been shown to affect bone marrow, lead to

hair loss, damage the mucous membranes of the gastrointestinal tract, and it is particularly toxic to the liver and kidneys.[15]

Medicinal applications for Pt metallodrugs are related to how they exert their anticancer effect in the body. It is well understood that the main target for Pt-based anticancer drugs is nuclear DNA. These compounds share a similar mechanism of action through the dissociation of labile ligand(s). The resulting open coordination site allows for Pt to complex to DNA. All three Pt compounds feature a square-planar geometry and the inclusion of leaving group ligands.[16] The first step is for the drug to be taken up by the cell. In the case of cisplatin, this is believed to be facilitated by copper transporters.[16,17] Next, aquation/activation takes place whereby a labile chloro ligand is replaced by a water molecule to form *cis*-$[Pt(NH_3)_2Cl(H_2O)]^+$.[16,18] From there, aquated cisplatin can enter the nucleus. Then, the aqua ligand dissociates and the drug binds to the purine bases of DNA: guanine and adenosine.[16,18] Following substitution of the second chloro ligand, the drug binds to another guanine base which causes DNA cross-linking. This prevents DNA transcription and translation which leads to cell death.[16,18]

Limitation of Platinum-based Chemotherapies

Given the cytotoxic properties of the aforementioned Pt compounds, their use as cancer treatments is a significant achievement in the field of medicinal inorganic chemistry. However, the potential for Pt compounds to be used in chemotherapy is curbed due to many cancers developing resistance to these types of drugs.[5] Thus, some Pt chemotherapeutics like oxaliplatin are often given in combination with other anticancer drugs, like fluorouracil.[19] To combat resistance to Pt chemotherapies and generate alternatives with milder side effect profiles, chemists have worked to expand the scope of potential metallodrug candidates to other elements in the d-block.

Expanding the Scope of Inorganic Anticancer Compounds

One of the most promising alternatives to Pt in medicinal inorganic chemistry is ruthenium (Ru). Metal complexes supported by Ru offer a few advantages to Pt. Two of the most important considerations are cost and toxicity. Ru is significantly less expensive than Pt. As such, metallodrugs which incorporate Ru centers should theoretically be more cost-effective than their Pt counterparts. In addition, as mentioned by Bergamo and Sava, Ru-based complexes are generally less toxic than Pt which can reduce the potential for chemotherapy-related side effects.[20] Given that Ru is lower cost and less toxic relative to Pt, it is a metal worth pursuing as a Pt alternative in metal-based chemotherapy drugs.

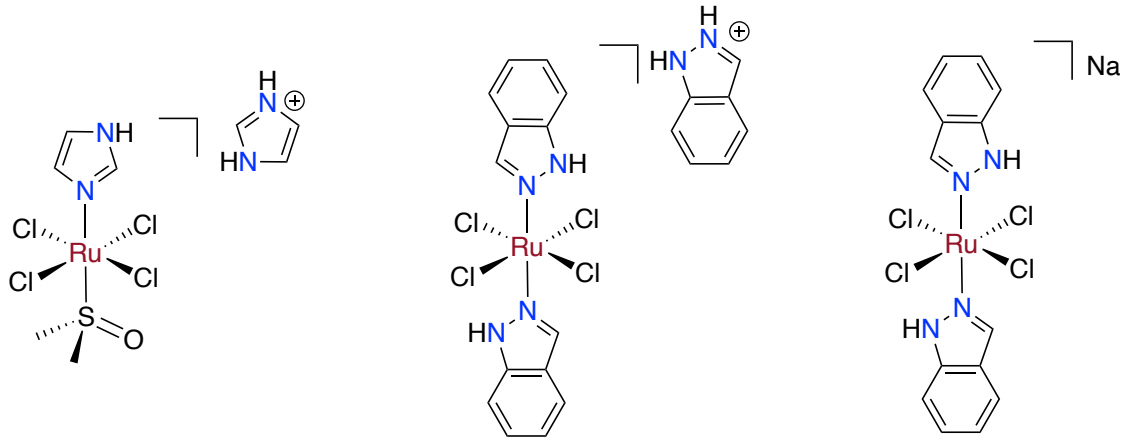

Figure 2. Examples of ruthenium complexes which have advanced to clinical trials. NAMI-A, KP1091, and KP1339 are all examples of metal complexes supported by Ru(III) centers. These complexes have been investigated for their anticancer properties. However, these three drug candidates have not made it to market due to undesirable properties including side effects.

Ruthenium-based Anticancer Compounds

Several Ru complexes have undergone or are currently being evaluated in clinical trials. These compounds are shown in Figure 2. NAMI-A initially failed to move beyond phase II clinical trials due to side effects.[21–23] However, it has been further evaluated in combination

treatments.[23,24] Another compound, KP1019, failed to advance through clinical trials because it was not very water soluble.[23,25,26] The poor solubility of KP1019 was improved by generating an analogue, KP1339.[23,27]Additionally, it is worth noting that NAMI-A, KP1019, and KP1339 are all Ru(III) complexes. It is believed that these complexes act as prodrugs and are reduced from Ru(III) to Ru(II) in cellular environments.[25,28] Therefore, the active form of NAMI-A, KP1019, and KP1339 is when the Ru center is in the +2 oxidation state.

Unlike Pt-based chemotherapeutics which are known to target DNA, the mechanism of action of Ru complexes in tumor suppression is less well understood. As outlined by Lin and colleagues, it is believed that Ru complexes exhibit their cytotoxic effect through multiple mechanisms of action (Figure 3).[23] It has been demonstrated that some Ru-based metallodrugs may kills cells by targeting DNA and blocking the cell cycle during S-phase.[23,29–31] Other reports suggest that Ru complexes target organelles. For instance, some work has found that Ru complexes may target mitochondria.[23,32–34] In addition, other findings suggest that the endoplasmic reticulum is a target of some Ru complexes.[23,35] The aforementioned targets for Ru compounds are not an exhaustive list. Rather, it describes a few notable examples which have been reported in the literature. The multiple cellular targets of Ru complexes may allow them to be less susceptible to drug resistance compared to Pt-based chemotherapies since Pt drugs primarily target DNA.

While the preliminary results of Ru compounds as chemotherapy drugs candidates are promising, they are not ideal since they do not selectively target cancer cells.[36] As mentioned before, one of the major hurdles in developing more organometallic chemotherapy drugs is the issue of selectivity. Ideally, a drug should be selective for its target to minimize potential side effects. In other words, a chemotherapy drug should be selective for cancerous cells while not

targeting healthy cells. For example, cisplatin is cytotoxic to cancer cells because it cross-links DNA. However, cisplatin lacks selectivity for cancer cells, and it is also cytotoxic to many non-cancerous cell types.[15]

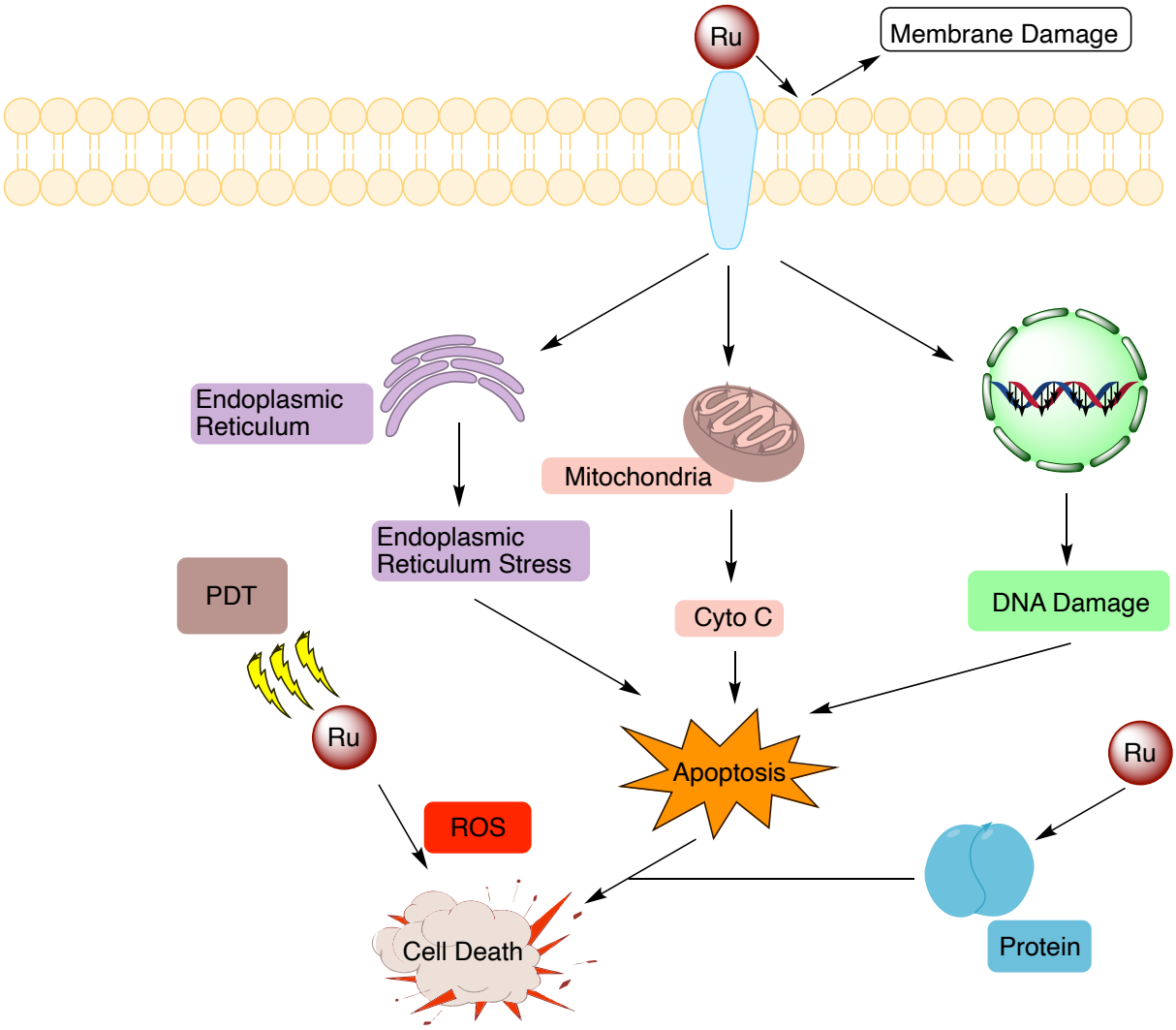

Figure 3. Cellular targets of ruthenium complexes. Ru complexes are known to target a variety of cellular structures and organelles. Some Ru-based drug candidates are cytotoxic by interacting with DNA which can lead to DNA damage and eventual cell death. Other Ru complexes target the endoplasmic reticulum or mitochondria. In addition, some Ru complexes can target proteins or the cellular membrane, which may lead to further damage. Lastly, a few Ru complexes can interact with light and potentially be used in PDT (photodynamic therapy). This figure was adapted from Lin and colleagues.[23]

Though much work is being done to address the selectivity of traditional organometallic drugs used in cancer treatment, there is growing interest in a different treatment modality where the cytotoxicity of a metallodrug can be modulated both spatially and temporally through the application of light. To this end, metal complexes supported by Ru are being investigated due to their desirable chemical and photophysical properties. This approach has the potential to be as efficacious as Pt-based anticancer drugs, while reducing the severity of side effects by employing a unique mechanism of action.

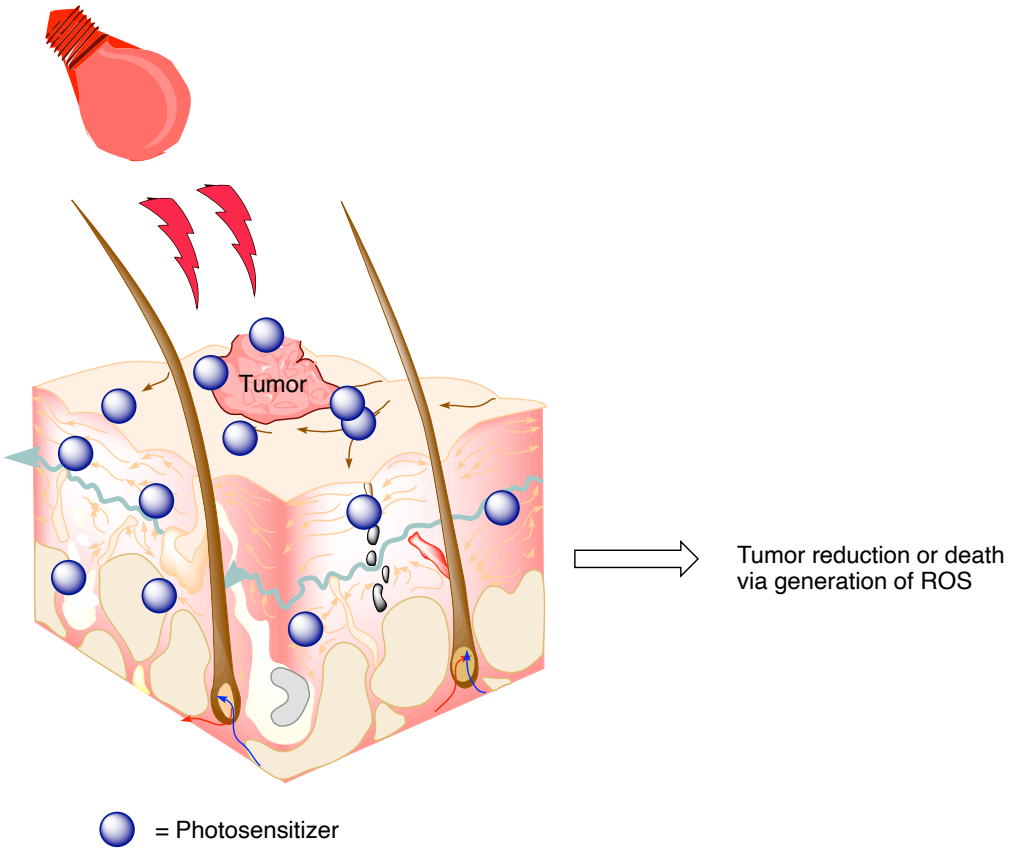

Figure 4. Photodynamic therapy applied to tumor treatment. This diagram shows how PDT can be used to treat a tumor. A photosensitizer (PS) is first given which can accumulate in a tumor and surrounding tissue. Next, light is applied to the area of the tumor. The PS reacts with light to generate reactive oxygen species (ROS). The ROS that are produced result in oxidative damage and can lead to cell death, thereby killing the cancerous cells that make up the tumor. This figure was adapted from Rui and colleagues.[37]

Photodynamic Therapy as an Alternative Approach

In an effort to create a metal antitumor drug with enhanced selectivity for cancerous cells, researchers have focused on developing a new class of drugs. PDT is a type of treatment most often used in cancer therapies. PDT uses light and a molecule that can act as a photosensitizer (PS).[38] As outlined by Abrahamse and colleagues, PDT relies on the "damage or destruction of living tissue by visible light in the presence of a photosensitizer and oxygen," which is referred to as the photodynamic effect.[7,39] Thus, the cytotoxicity of a PS molecule can be "turned on" in the presence of light and "turned off" or greatly reduced without the application of light (Figure 4). In doing so, the cytotoxic drug is mostly localized in the area exposed to light, as opposed to the systemic cytotoxicity of traditional treatments.

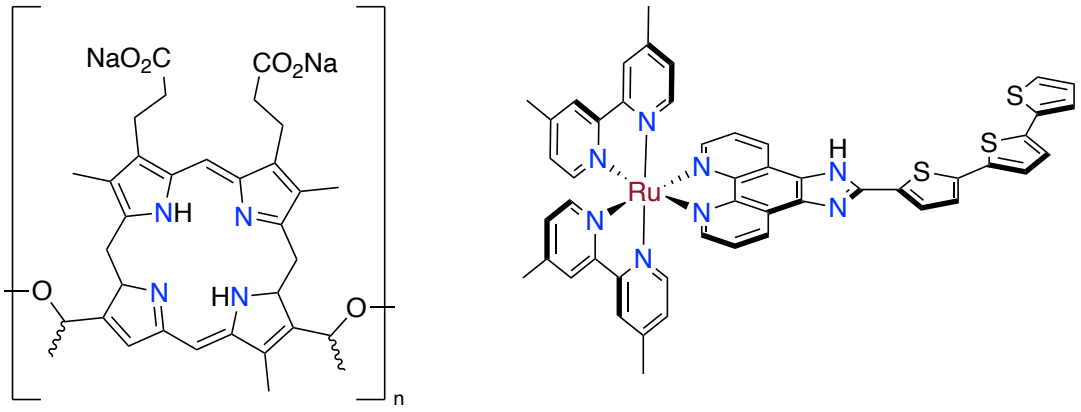

Photofrin **TLD1433**

Figure 5. Examples of photosensitizers for cancer treatment. The structures of two PS, Photofrin and TLD1433, are shown. Photofrin is one of the most used PS for PDT. The structure of Photofrin was adapted and modifed from Josefsen and Boyle.[40]

Clinical Uses of PDT

Clinically, PDT has been applied to treat a number of different types of cancer. One of the first PS that was granted FDA approval is Photofrin (Figure 5). This drug is used in PDT for the treatment of esophageal cancer and early non-small cell lung cancer.[41] In recent years, new photosensitizers have been developed which has expanded the scope of indications that can be treated with PDT to include basal cell carcinoma, squamous cell carcinoma, and bladder cancer, just to name a few.[42,43] The three compounds that have been approved by the FDA for PDT in cancer are based on porphyrin and porphyrin derivatives. One limitation of these compounds is that they are excited by shorter wavelengths of light near the UV region. More structurally diverse compounds based on Ru(II) have been investigated to shift the wavelength of light needed to excite these PS to the visible or near-infrared region.[7]

Type I and Type II Mechanisms

As mentioned previously, PDT consists of three elements: a PS, light (which is of a specific wavelength), and oxygen (O_2).[44,45] This point is important to emphasize because it relates to how a PS is able to produce ROS, which is termed the photodynamic effect, as well as the underlying photophysical and chemical mechanisms that govern its efficacy. Based on the photodynamic effect, photoreactions for PDT can be classified as either following a type I or type II mechanism. The distinction between these two types of mechanisms is based on what type of ROS is produced.

PDT begins with the administration of a PS that is distributed to the tissue of interest. Next, light is applied to the tissue and is absorbed by the PS, thereby initiating the photodynamic effect. When the PS absorbs energy from a specific wavelength of light, one of its electrons is promoted from its singlet ground state (^1PS) to the singlet excited state ($^1PS^*$), as illustrated in the

Jabłonski diagram (Figure 6).[7,46,47] From there, the system can reach a more stable electronic state through intersystem crossing to the triplet excited state ($^3PS^*$) which requires the electron to undergo spin conversion (Figure 6).[7,48] The type of molecule to which $^3PS^*$ transfers energy to determines whether the photodynamic effect follows a type I or type II mechanism.[47] Regardless of the type of mechanism, the photodynamic effect produces ROS such as singlet oxygen ($^1O_2$), hydroxyl radical ($HO^\bullet$), or hydrogen peroxide (H_2O_2) which result in oxidative damage, thereby killing the cell.[44] As reported by Rocha, the quantum yield of $^3PS^*$ is an important factor in determining the production of $^1O_2$.[49] Thus, an ideal photophysical property for a PS is that it has a high quantum yield since it is related to the generation of $^1O_2$ and other ROS.[7]

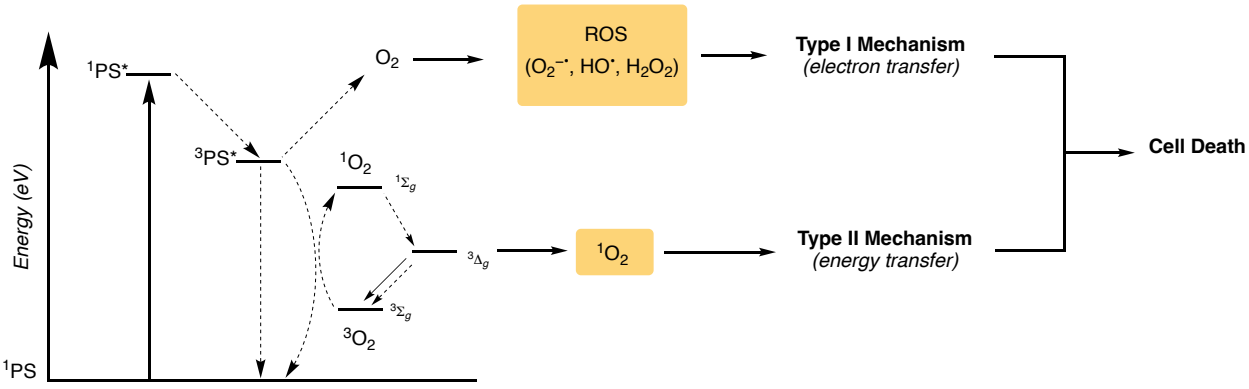

Figure 6. Jabłonski diagram depicting the photodynamic effect. The Jabłonski diagram illustrates how a PS absorbs energy from light and is promoted from ^1PS to $^1PS^*$. The PS then undergoes intersystem crossing to reach $^3PS^*$. The molecule to which $^3PS^*$ transfers energy to determines whether the mechanism is type I or type II. Fluorescence and phosphorescence labels have been omitted for clarity. The diagram is an adapted version from the works of Monro and Correia.[7,45]

If the photodynamic effect follows a type I mechanism, photoinduced electron transfer occurs which produces radicals. If these radicals are in the presence of O_2, they can generate ROS like $O_2^{-\bullet}$, $HO^\bullet$, and H_2O_2.[7,45,49] In a type II mechanism, $^3PS^*$ transfers energy to O_2, which is in the triplet ground state. This energy transfer produces highly reactive $^1O_2$, leading to oxidative damage.[7,45,49] One similarity between the pathways is that they both require O_2 to produce ROS.

It has been reported that of these two pathways, the type II mechanism occurs more frequently.[45,49] Though both type I and type II are expected to occur at the same time, they are influenced by O_2 concentration and the type of PS that is used.[45,47,48,48]

The benefit of PDT is that ROS are short-lived so much of the oxidative damage that leads to cell death occurs in a limited area. This is one of the ways PDT differs from traditional chemotherapies because the cytotoxic agent is restricted spatially to the area where light is applied. In addition, PDT tends to cost less and leads to less tissue scarring compared to other treatments.[50,51] However, PDT has some drawbacks that has limited its clinical scope to certain types of cancer. For example, PDT is not an efficient methods of treating cancers that have spread to other tissues.[45,50] Further, the ability of the photodynamic effect to generate oxidative damage through ROS is limited because light cannot penetrate tissue very well.[45,50,52] Therefore, PDT is generally reserved for tumors that are located superficially on tissues.

Ruthenium Complexes Explored for PDT

Though much of the work on PS has been with organic molecules like porphyrin or porphyrin derivatives, some researchers have focused on expanding the structural diversity of these compounds to shift their absorbance from the near UV into the visible to near-infrared regions. In recent years, effort has been made to synthesize PS for use in PDT that are supported by transition metals. Complexes supported by d-block transition metals offer several features that make them attractive PS candidates. Altering the oxidation state, changing the geometry around the metal center, water solubility, and ligand tunability are just some parameters that can be modified to enhance chemical and photophysical properties of a PS supported by a metal.[7,53–55] One of the metals that has perhaps received the most attention for this endeavor is Ru.

Ru compounds have gained attention because they can potentially supplant traditional Pt-

based chemotherapies for the treatment of certain types of cancer. For instance, Ru complexes are expected to be just as efficacious as Pt anticancers, but with less toxicity and a higher degree of selectivity, thereby reducing possible side effects.[23,56–58] In addition, the cytotoxicity of different Ru compounds is expected to have multiple mechanisms of action as shown in Figure 3. Lastly, there is more robust literature examining how Ru complexes can function as PS compared to Pt.[7,23]

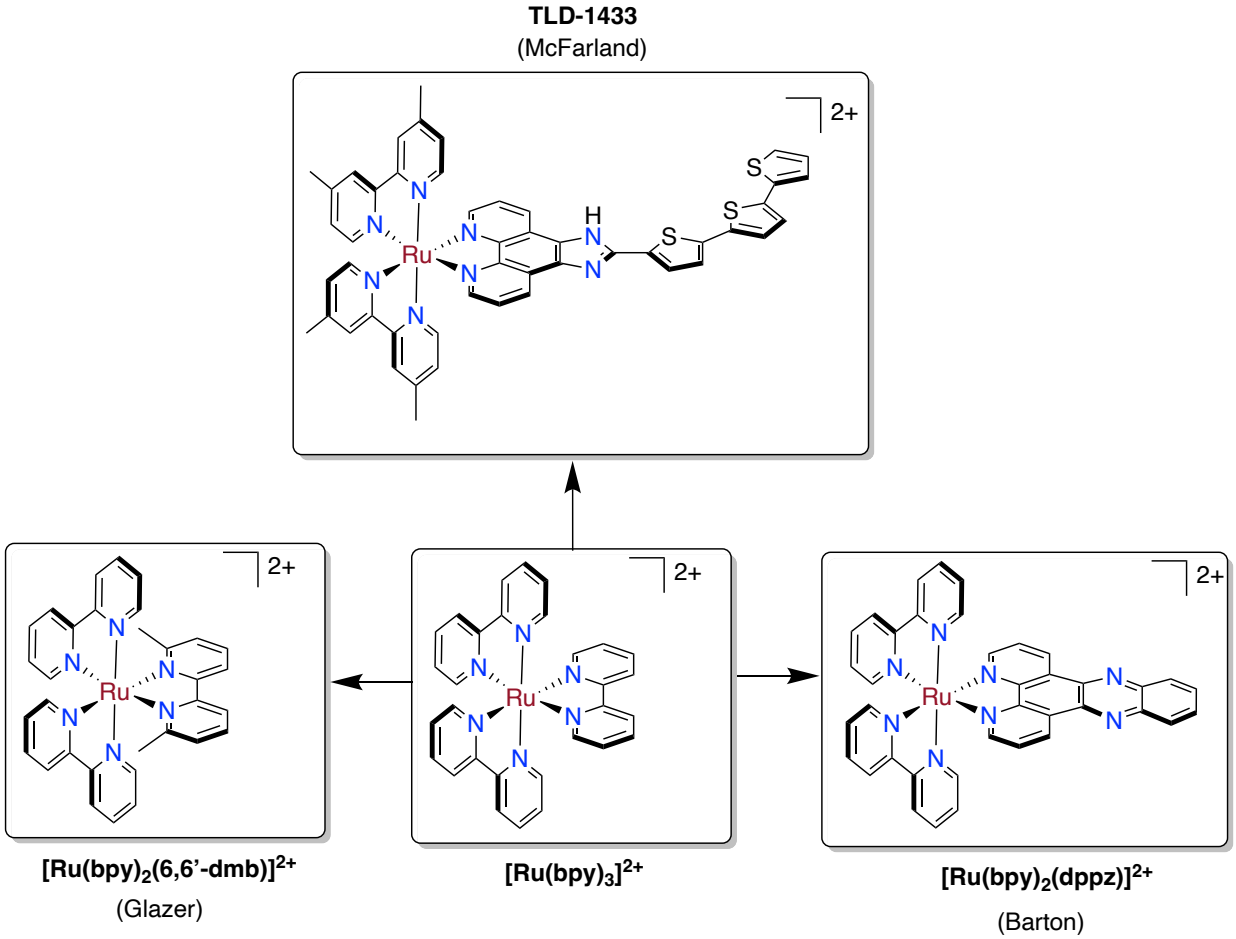

Scheme 1. Examples of ruthenium(II) complexes that function as photosensitizers. The compound $[Ru(bpy)_3]^{2+}$ is one of the most well know and characterized Ru(II) PS. This compound has led to the rise of other PS like $[Ru(bpy)_2(dpzz)]^{2+}$ and $[Ru(bpy)_2(6,6'\text{-dmb}]^{2+}$. TLD-1433 is a Ru(II) complex which is currently being explored in clincal trials as a potential cancer treatment. The following figure is adapted from the work of Monro and colleagues.[7]

Ru is an attractive metal to support complexes that can function as a PS due to its intrinsic chemical and photophysical properties. As described by Monro and colleagues, the literature on Ru(II) PS systems is well established.[7] Thus, a metal complex containing a Ru(II) center is worth pursuing due to the precedent of it potentially functioning as a PS. Further, Aksakal and coworkers note that the work on Ru(II) complexes with photosensitizing properties has primarily focused on systems supported by polypyridyl ligands.[33,59–61] Polypyridyl ligands are N-heterocycles with conjugated π electrons. The electronic structure of this ligand system is important for how Ru(II) complexes interact with light. As Aksakal and coworkers describe, Ru(II) polypyridyl-based complexes are of interest because they have "long emission state lifetimes from the triplet metal-to-ligand charge transfer state (MLCT)" that are quenched by $^3O_2$ (triplet oxygen) which result in a high $^1O_2$ quantum yield.[33,59,61,62] These photophysical characteristics reflect why Ru(II) complexes may function as effective photosensitizers and why Ru(II) is of great interest.

When designing our complex, it was important to examine previous work on Ru(II) systems with PS properties as inspiration and to better inform potential synthetic avenues. As previously mentioned, much of the literature on Ru(II) PS has been based on the polypyridyl complex, $[Ru(bpy)_3]^{2+}$ (where bpy = 2,2'-bipyridine) and its structural analogues (Scheme 1). The chemistry around $[Ru(bpy)_3]^{2+}$ and its photophysical properties are well documented.[7,63–65] When $[Ru(bpy)_3]^{2+}$ is excited with ~420 nm light, it has a ^{3}MLCT lifetime of ~200 ns and 1 μs in aerated acetonitrile (MeCN) and deoxygenated MeCN, respectively.[7,64,66] The shorter excited state lifetime of $[Ru(bpy)_3]^{2+}$ in aerated solvent can be rationalized through quenching of the excited state via $^3O_2$. Another important photophysical parameter of a PS is its quantum yield. It was reported that $[Ru(bpy)_3]^{2+}$ had an emissive quantum yield (Φ_{em}) of 10% in deoxygenated

MeCN and a quantum yield of $^1O_2$ production (Φ_Δ) of 56% in aerated MeCN.[7,67,68] These photophysical values are important to consider because they can quantify the potential effectiveness of a PS. According to Monro et al., other notable properties of a good photosensitizer to consider are as follows: high quantum yield for $^1O_2$ production (Φ_Δ), molar extinction coefficient in the PDT window of ~700–900 nm, and solubility in aqueous environments.[7]

Since the synthesis and characterization of $[Ru(bpy)_3]^{2+}$, a compound that can function as a PS and is capable of generating $^1O_2$ when irradiated with light, more complexes supported by Ru(II) center(s) have been reported. One of these Ru compounds, TLD-1433 is an investigational drug that is currently being evaluated in clinical trials as a PS for bladder cancer (Scheme 1).[7] Other examples of Ru(II) complexes are illustrated in Scheme 1 and were also highlighted in a review by Monro and coworkers.[7] The Barton group first reported $[Ru(bpy)_2(dppz)]^{2+}$ (where dppz = dipyrido[3,2-a:2',3'-c]phenazine). This compound was shown to behave as a molecular light switch for DNA, indicating an interaction between the Ru(II) complex and DNA.[69] Another example of a Ru PS was reported by the Glazer group. The complex, $[Ru(bpy)_2(6,6'\text{-dmb}]^{2+}$ (where 6,6'-dmb = 6,6'-dimethyl-2,2'-bipyridine), was cytotoxic upon irradiation with light.[70,71] While these structures are seemingly diverse, they are all derivatives of $[Ru(bpy)_3]^{2+}$ and feature polypyridyl moieties. Therefore, more work can be done to examine the effect of ligands on these PS.

Preliminary Studies

Before the work could be begin, we first needed to select an organic scaffold to support a Ru(II) center. The Lee Lab has a history of using a tridentate system, $HCz^{tBu}(Pyr^R)_2$ (R = H (**1**), Me (**2**), iPr (**3**)). $HCz^{tBu}(Pyr^R)_2$ is a tridentate redox non-innocent N,N,N-pincer ligand (Figure 7).

Further, we have had success in generating a series of metal complexes using this ligand system with applications toward C–H activation,[72] dinitrogen (N_2) activation,[73–76] and catalytic hydrosilylation.[77] Our ligand system is based on a carbazole backbone and is also tunable at positions *a*, *b*, and *c* (Figure 7).

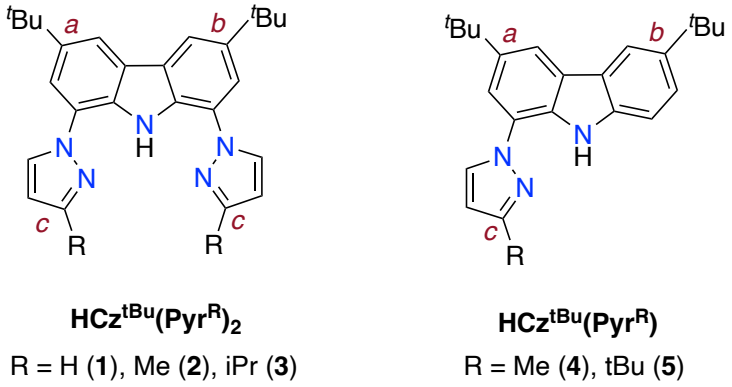

HCz^{tBu}(Pyr^{R})$_2$
R = H (**1**), Me (**2**), iPr (**3**)

HCz^{tBu}(Pyr^{R})
R = Me (**4**), tBu (**5**)

Figure 7. Tridentate N,N,N-pincer and bidentate N,N-ligand systems. HCz^{tBu}(Pyr^{R})$_2$ (R = H (**1**), Me (**2**), iPr (**3**)) and HCz^{tBu}(Pyr^{R}) (R = Me (**4**), tBu (**5**)) will be investigated in this work. The ligands are tunable at position *a*, *b*, and *c* which allows for modification of chemical and photophysical properties in the future.

The tunability of our ligand allows us to conduct structure–activity relationship studies in the future to probe chemical and photophysical properties like absorbance and solubility. Further, HCz^{tBu}(Pyr^{R})$_2$ (R = H (**1**), Me (**2**), iPr (**3**)) contains nitrogen-donating ligands, which is a well-defined structural motif in established PS that are supported by a Ru center. One important photochemical property of a PS to consider is quantum yield. As mentioned previously, a PS that has a high quantum yield is ideal because this value is related to the generation of $^1O_2$ and other ROS.[7] In the case of our design, we note that the carbazole backbone of our ligand platform is more chemically rigid than the polypyridine of established PS. One of the predictors of molecules with higher quantum yield is that they are structurally rigid.[78] Given that our ligand is

more structurally rigid than polypyridine, the effect of rigidity on its photophysical properties merits study.

In addition, we want to expand the scope of this project by using a bidentate system which is based on our established tridentate N,N,N-pincer ligand, $HCz^{tBu}(Pyr^{R})_2$ (R = Me (**4**), tBu (**5**)). The bidentate ligand system is less bulky than the tridentate ligand. Thus, we hope to synthesize more diverse structures like a homoleptic complex coordinated by three bidentate N,N- ligands, which are not possible with the tridentate N,N,N-pincer ligand.

Thesis Objectives

The objective of this thesis is to examine whether our tridentate N,N,N-pincer and bidentate N,N ligand systems can be used to support Ru-based metal complexes. Herein, we will describe the synthesis and characterization of two novel Ru(II) complexes. In the future we hope to create more diverse Ru(II) complexes using our ligand system. In addition, we hope to find a collaborator who can assist in photophysical measurements of our complexes to assess their potential as PS.

CHAPTER II

MATERIALS AND METHODS

Overview

All reactions and analyses were performed using commercially available reagents. All reactions were performed using glassware that had been dried overnight at 150 °C. Ligand syntheses were performed in a Schlenk line under inert N_2 atmosphere. Syntheses of metal complexes were performed in a M. Braun UNIlab Pro glovebox under inert N_2 atmosphere. All solvent used in the glovebox was degassed and purified via a Pure Process Technology solvent purifier. Before use, a sample of each solvent was tested for the presence of O_2 using a drop of sodium benzophenone ketyl in tetrahydrofuran (THF). ^{1}H NMR (nuclear magnetic resonance) data were obtained on a Bruker Avance III HD 500 MHz spectrometer at 25 °C. ^{1}H NMR spectra were referenced to the following solvent peaks: acetone-d^6 at $\delta = 2.04$ ppm, C_6D_5H at $\delta = 7.16$ ppm, $CDCl_3$ at $\delta = 7.24$ ppm. Cyclic voltammetry (CV) data were obtained on a CH-Instruments electrochemical analyzer (model 620E). CV measurements were performed with 1 mM solutions of analyte and 0.1 M $(n\text{-Bu})_4NPF_6$ in a 50:50 mixture of toluene and THF. CV measurements were obtained using a 3 mm glassy carbon working electrode, a platinum wire counter electrode, and a pseudo reference electrode of silver wire. UV-Visible (UV-Vis) spectroscopy was performed using an Agilent Technologies Cary 8454 UV-Vis by creating 1 mM solutions of analyte dissolved in MeCN or a 50:50 mixture of MeCN and toluene. Crystallographic data were gathered using a Bruker AXS D8 Quest diffractometer with a PhotonII charge-integrating pixel

array detector. Crystallographic parameters are presented in Appendix A.

Synthesis of HCz^{tBu}(Pyr^{H})$_2$ (1)

To a 500 mL, three-neck round-bottom flask was added 9.53 g (26.2 mmol) 1,8-Dibromo-3,6-*tert*-butyl-9*H*-carbazole, 7.8 g (114 mmol) of 1*H*-pyrazole, 12.8 g (114 mmol) of potassium *tert*-butoxide (*t*-BuOK), and 2.3 g (20 mmol) of *N,N,N,N*-tetra-methyl-ethylenediamine (TMEDA). The reagents were dissolved in 150 mL dimethylformamide (DMF). Five freeze-pump-thaw cycles were done to degas the yellow slurry. 2.9 g (20 mmol) of copper(I) oxide (Cu_2O) was added and the reaction was refluxed at 150 °C for 5 days under inert N_2 atmosphere. The resulting brown slurry was dissolved in 200 mL dichloromethane (DCM) and washed with 3x200 of 1M HCl (hydrochloric acid), 3x200 mL of 1 M NH_4OH (ammonium hydroxide), and 2x200 mL of 1 M NH_4Cl (ammonium chloride) solutions. The DCM layer was collected, dried using $MgSO_4$ (magnesium sulfate), and the solvent was removed by rotary evaporation. The resulting brown solid was purified using silica gel column chromatography with toluene as the mobile phase solvent. The mobile phase was collected, and toluene was removed by rotary evaporation. The resulting light brown solids were crystallized from a concentrated *n*-hexane solution at −20 °C to yield the product as off-white solids (4.9 g, 52%). ^{1}H NMR (500 MHz, $CDCl_3$, δ): 1.52 ($C(CH_3)_3$, s, 9H), 6.57 (ArH, s, 1H), 7.59 (ArH, s, 1H), 7.91 (ArH, s, 1H), 8.07 (ArH, s, 1H), 8.15 (ArH, s, 1H), 11.27 (NH, s, 1H).

Synthesis of HCz^{tBu}(Pyr^{tBu}) (5)

To a 500 mL, three-neck round-bottom flask was added 9.53 g (26.2 mmol) 1-Bromo,3,6-di-*tert*-butyl-9*H*-carbazole, 9.91 g (79.8 mmol) 3-*ter*t-butylpyrazole, 4.95 mL (3.85 g, 33.1 mmol) of TMEDA, 8.95 g (79.8 mmol) of *t*-BuOK. The reagents were dissolved in 250 mL DMF. The yellow slurry was degassed by three cycles of freeze-pump-thaw. Next, 5.71 g (39.9

mmol) of Cu_2O was added. The slurry was then refluxed for 3 days at 150 °C under inert N_2 atmosphere. After the reaction was complete, the resulting brown slurry was added to a separatory funnel along with 250 mL of diethyl ether. The solution was then washed with 3x50 mL of 1 M HCl, 3x50 mL of 1 M NH_4OH, and 3x50 mL of 1 M NH_4Cl. The diethyl ether layer was collected and dried over $MgSO_4$. Solvent was removed by rotary evaporation, leaving behind an off-white solid. The resulting solid was recrystallized from a concentrated *n*-hexane solution at −20 °C to yield the product as an off-white solid (9.35 g, 88%). ^{1}H NMR (500 MHz, $CDCl_3$, δ): 1.48 (9H, s, $C(CH_3)_3$), 1.49 (9H, s, $C(CH_3)_3$), 1.50 (9H, s, $C(CH_3)_3$), 6.40 (1H, d, ArH), 7.42 (1H, dd, ArH), 7.49 (1H, d, ArH), 7.53 (1H, dd, ArH), 7.99 (1H, d, ArH), 8.06 (1H, d, ArH), 8.11 (1H, d, ArH), 10.04 (1H, br, NH).

Synthesis of $(Cz^{tBu}(Pyr^H)_2)_2Ru$ (6)

To 87.4 mg (0.21 mmol) of $HCz^{tBu}(Pyr^H)_2$ dissolved in THF at ambient temperature under inert N_2 atmosphere was added 23.6 mg (0.22 mmol) of lithium diisopropylamide (LDA). The resulting solution became fluorescent and was stirred for 1 hour. The fluorescent solution was then added to a suspension of 32.1 mg (0.054 mmol) $[Ru(p\text{-cymene})Cl_2]_2$ in THF and stirred overnight at ambient temperature. The solvent was removed in vacuo to produce a red solid. The solid was dissolved in toluene before filtration over a Celite pad. Toluene was removed under reduced pressure leaving behind a red solid. Pentane was added to the solid to form a slurry and was filtered over a Celite pad. The solid was dissolved using toluene and the resulting solution was dried using reduced pressure to yield the final product. Red crystals suitable for X-ray diffraction were grown in toluene at −20 °C (88.1 mg, 37%). ^{1}H NMR (500 MHz, C_6D_6, δ): 1.55 (s, 36H, $C(CH_3)_3$), 5.17 (t, 4H, J = 0.99, ArH) 6.88 (d, 4H, J = 0.97, ArH), 7.46 (s, 4H, J =1.02, ArH), 7.59 (s, 4H, J = 1.03, ArH), 8.69 (s, 4H, J = 1.00, ArH).

Synthesis of $Cz^{tBu}(Pyr^{H})_2RuCl(PPh_3)_2$ (7)

To 32.0 mg (0.0778 mmol) of $HCz^{tBu)}(Pyr^{H})_2$ dissolved in THF at ambient temperature under inert N_2 atmosphere was added 9.1 mg (0.0850 mmol) of LDA. The resulting solution became fluorescent and was stirred for 1 hour. The fluorescent solution was then added to 74.5 mg (0.0778 mmol) $RuCl_2(PPh_3)_3$ suspended in THF and stirred overnight at ambient temperature. The solvent was removed in vacuo to produce a red solid. The red solid was dissolved in toluene before filtration over a Celite pad. Toluene was removed under reduced pressure leaving behind an oily, red solid. Pentane was added to the solid to form a slurry and the solid was filtered over a Celite pad. The solid was dissolved using toluene and the resulting solution was dried using reduced pressure to yield the final red product. Red crystal suitable for X-ray diffraction were grown in toluene at −20 °C (81.9 mg, 98% quantitative yield). ^{1}H NMR (500 MHz, C_6D_6, δ): 1.39 (s, 18H, $C(CH_3)_3$), 5.80 (d, 2H, *J* = 1.00, ArH), 6.77 (d, 2H, *J* = 1.91, ArH), 7.28 (s, 15H, *J* = 2.31, ArH), 7.57 (s, 2H, *J* = 1.12, ArH), 7.74 (s, 2H, *J* = 1.09, ArH) 9.10 (s, 2H, *J* = 1.00, ArH).

CHAPTER III

RESULTS AND CONCLUSIONS

We hypothesize that our established tridentate ligand, $HCz^{tBu}(Pyr^{R})_2$ (R = H (**1**), Me (**2**), iPr (**3**)), could be applied to produce a series of metal complexes supported by a Ru(II) center. Specifically, we want to synthesize a homoleptic complex based on the following formula: $(Cz^{tBu}(Pyr^{R})_2)_2Ru$. Our lab has had success in characterizing homoleptic complexes using first-row transition metals that are supported by $HCz^{tBu}(Pyr^{H})_2$. The Lee lab has reported a homoleptic complex that features an iron (Fe) center, which is in same group as Ru. The electronic and redox properties of this Fe(II) complex have been studied in depth and manuscripts are being prepared for publication. We have synthesized more examples of homoleptic complexes of the form $(Cz^{tBu}(Pyr^{H})_2)_2M$ (M = metal) using other first-row transition metals including cobalt (Co), nickel (Ni), and zinc (Zn). Given the precedent of our established N,N,N-pincer ligand platform to support homoleptic complexes, we apply the same synthetic techniques to produce a homoleptic compound that features a Ru(II) center. We directed our focus on Ru complexes because they can potentially function as a PS.[7] Further, we want to see if ligands **2** or **3** can be used to generate homoleptic complexes to examine how using more electron-donating substituents on the pyrazole arms influence the chemical and photophysical properties of the resulting complexes that are formed. Before this work could begin, we first had to synthesize the tridentate ligand, $HCz^{tBu}(Pyr^{R})_2$ (R = H (**1**), Me (**2**), iPr (**3**)). In addition we also produced a bidentate ligand in the form $HCz^{tBu}(Pyr^{R})$ (R = Me (**4**), tBu (**5**) since bidentate ligands have been

used to support Ru(II) PS in the past.[7]

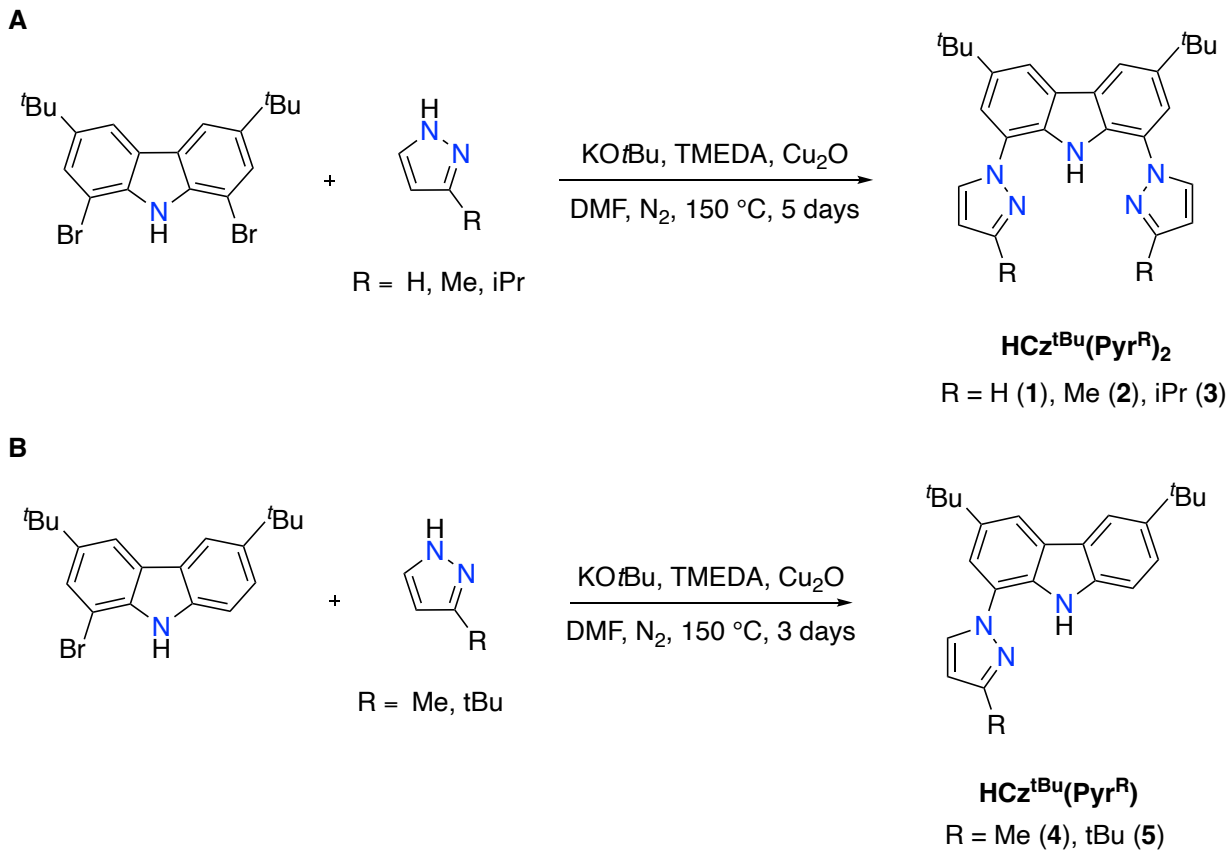

Scheme 2. Synthesis of ligands 1–5.

Generation of Carbazole-based Ligand Platform

The synthesis and characterization of **1–5** has been covered by our lab in previous work.[72–77] The conversion of staring material to ligand is based on a modified procedure from the literature.[79] For ligands **1–3**, 1,8-dibromo-3,6-*tert*-butyl-9H-carbazole is refluxed with a pyrazole (or a pyrazole derivative), KO*t*Bu, TMEDA, and Cu_2O to produce a N,N,N-pincer ligand (Scheme 2A). Upon deprotonation, $HCz^{tBu}(Pyr^{R})_2$ is converted to $Cz^{tBu}(Pyr^{R})_2^-$, which coordinates to metal centers meridionally through a tridentate binding mode. Using a procedure modified from the synthesis of our tridentate ligands, the bidentate ligands **4–5** can be produced

(Scheme 2B). With compounds **1–5** synthesized, we first set out to produce a homoleptic Ru(II) complex using our tridentate ligand system (**1-3**).

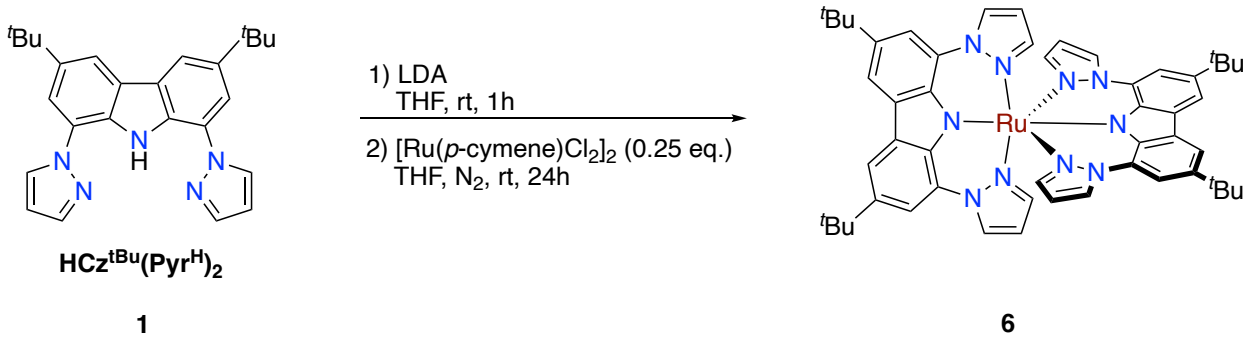

Scheme 3. Synthesis of complex 6.

Synthesis and Characterization of Complex 6

The compound described herein is a homoleptic complex supported by a Ru(II) center. The synthesis of **6** is outlined in Scheme 3. Complex **6** is generated through the deprotonation of $HCz^{tBu}(Pyr^{H})_2$ by LDA to produce the deprotonated form, $Cz^{tBu}(Pyr^{H})_2^{-}$. Next, the deprotonated ligand undergoes transmetalation through the addition of 0.25 equivalents of $[Ru(p\text{-cymene})Cl_2]_2$ at ambient temperature under inert N_2 atmosphere (Scheme 3). ^1H NMR spectroscopy of **6** shows diamagnetic resonances which are in agreement with a d^6 low-spin Ru(II) center (Figure 13).

Crystal Structure of 6

Bright-red crystals of **6** were grown from a concentrated solution of toluene at –20 °C. The molecular structure of **6** was solved and is reported in Figure 8. The solid-state structure of **6** was found to be a homoleptic complex whereby one Ru(II) center is supported by two molecules of $Cz^{tBu}(Pyr^{H})_2^{-}$. The NNN-pincer ligands are oriented orthogonally around the Ru(II) center. The structure of **6** is consistent with analogous Fe(II), Co(II), Ni(II), and Zn(II) complexs supported by two $Cz^{tBu}(Pyr^{H})_2^{-}$ ligands previously reported by our group.[80] The bond angle

between the two carbazole nitrogens (N_{Cz} = N3, N8) and the Ru(II) center in **6** is 179° (Figure 8). Therefore, the geometry around the Ru(II) center in **6** is characterized as near-perfect octahedral geometry.

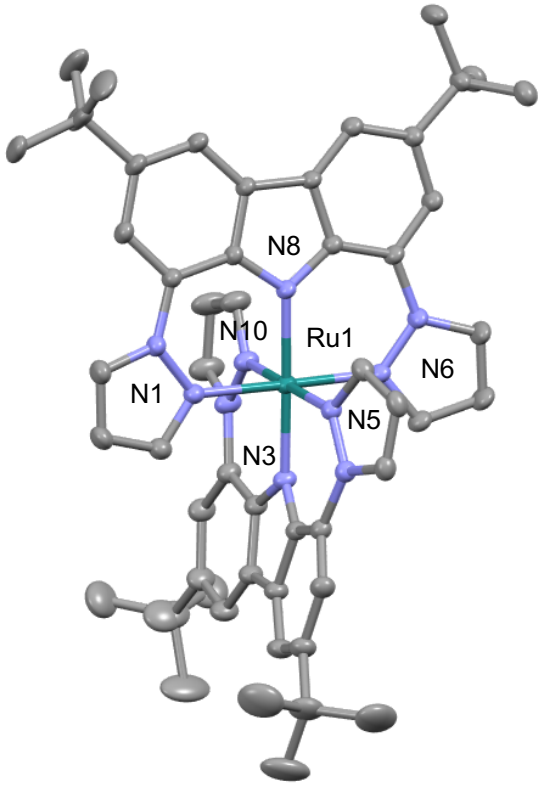

Figure 8. Molecular Structure of complex 6.

Selected bond lengths for complex **6** were collected and are reported in Table 1. As expected, the distance between the two carbazole nitrogens (N_{CZ}) are nearly identical. The distance between Ru1 to N3 and N8 was 2.025(1) Å and 2.022(1) Å, respectively. Further, the bond distances between the metal center and the pyrazole nitrogens (N_{Pyr}) in **6** were similar and are within ~0.010 Å of each other. The bond length averages of **6** are also compared to two complexes of the type $(Cz^{tBu}(Pyr^{H})_2)_2M$ reported by our group (Table 2).[80]

Number	Object 1	Object 2	Length (Å)
1	N10	Ru1	2.078(2)
2	N1	Ru1	2.069(2)
3	N8	Ru1	2.022(1)
4	Ru1	N6	2.073(2)
5	Ru1	N5	2.067(2)
6	Ru1	N3	2.025(1)

Table 1. Selected bond distances for complex 6. Bond lengths are reported in Angstroms (Å)

	$M–N_{CZ}$	$M–N_{Pyr}$
6	2.024(1)	2.072(2)
$(Cz^{tBu}(Pyr^{H})_2)_2Fe$	2.056(2)	2.218(2)
$(Cz^{tBu}(Pyr^{H})_2)_2Co$	2.016(1)	2.170(1)

Table 2. Average bond lengths of 6 compared to corresponding iron(II) and cobalt(II) complexes. Bond reported in Angstroms (Å). The bond length values for $(Cz^{tBu}(Pyr^{H})_2)_2Fe$ and $(Cz^{tBu}(Pyr^{H})_2)_2Co$ were reported by our lab.[80]

When compared to other analogous homoleptic complexes of Fe(II) and Co(II), the $M–N_{CZ}$ bond length average we observe in **6** are consistent. The $M–N_{CZ}$ bond length in **6** are shorter than $(Cz^{tBu}(Pyr^{H})_2)_2Fe$ and slightly longer than $(Cz^{tBu}(Pyr^{H})_2)_2Co$. For $M–N_{Pyr}$, the bond length averages are shorter in **6** than in $(Cz^{tBu}(Pyr^{H})_2)_2Fe$ or $(Cz^{tBu}(Pyr^{H})_2)_2Co$, likely due to the spin states.[80]

The bond distance values reported for **6** are consistent with those of other PS Ru(II) complexes that have been reported. For instance, in the archetype Ru(II) complex $[Ru(bpy)_3]^{2+}$, the Ru–N bond distance was found to be 2.057(3) Å .[81] This distance is ~0.02 Å longer than the

Ru–N_{Pyr} distance and is ~0.025 Å shorter than the Ru–N_{CZ} distance we report for complex **6**. In addition, the bond distances in **6** are in agreement with another Ru(II) complex that functions as a PS, $[Ru(phen)_2(bpy)]^{2+}$ (where phen = 1,10-phenanthroline). The Ru–$N_{bpy/phen}$ bond lengths for this compound range from 2.046(3) to 2.078(3) Å.[82,83] These distances are similar to the ones we report for **6**, further corroborating that the molecular structure of **6** is in line with similar PS in the $[Ru(bpy)_3]^{2+}$ family. With complex **6** in hand, we sought to investigate its photophysical and electronic properties through characterization via UV-Vis spectroscopy and CV.

UV-Visible Spectroscopy of 6

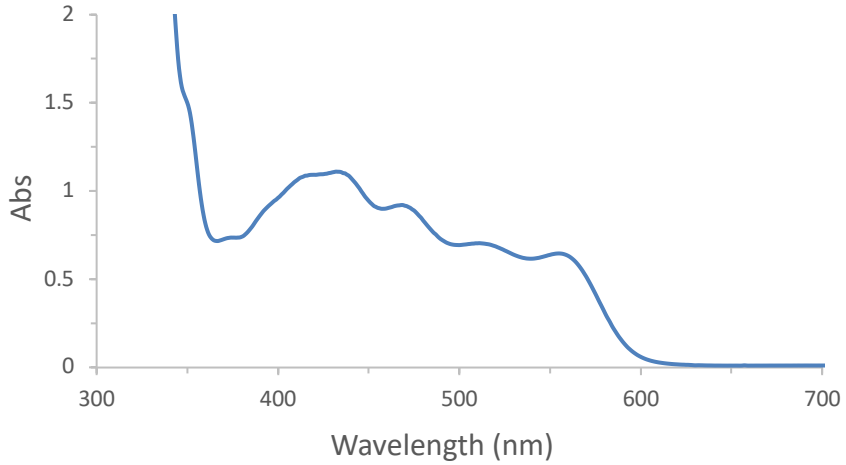

Figure 9. Absorption spectrum of 6. Absorption measurements are measured on a 1 mM solution of **6** in a 50:50 composition of MeCN and toluene.

UV-Vis spectroscopy was performed on **6** to further probe its electronic structure and potential ability to function as a PS. Absorption measurements were performed on a 1 mM solution of **6** in a 50:50 mixture of MeCN and toluene. The UV-Vis absorption spectrum of **6** (Figure 9) revealed features that are consistent with other Ru(II) PS. For instance, the absorption spectrum of **6** features a longest wavelength absorption maxima at 432 nm that tails to ~650 nm. This absorption band is a characteristic feature of Ru(II) complexes and represents ^{1}LC (singlet

ligand-centered) and singlet metal-ligand charge transfer (^{1}MLCT) transitions.[64,65] The absorption maxima at 432 nm we observe for **6** is consistent with the Ru(II) polypyridyl family of PS. For example, the parent compound $[Ru(bpy)_3]^{2+}$ has an absorption maxima at 450 nm.[84–87] Further, TLD1433 has a longest wavelength absorption maxima at 420 nm which was assigned to ^{1}LC and ^{1}MLCT transitions.[88] The absorbance maxima for **6** are slightly red-shifted compared to TLD1433 and more blue-shifted when compared to $[Ru(bpy)_3)^{2+}$. With respect to other established Ru(II) polypyridyl complexes, the absorption spectrum of **6** features a prominent absorption band observed throughout the visible region from ~365 to 600 nm. This spectral feature is broader than the absorption band for $[Ru(bpy)_3]^{2+}$ or TLD1433 within the same spectral region. The photochemistry of **6** merits further study as it suggests that the complex can be excited by wavelengths that are more red-shifted.

Cyclic Voltammetry of 6

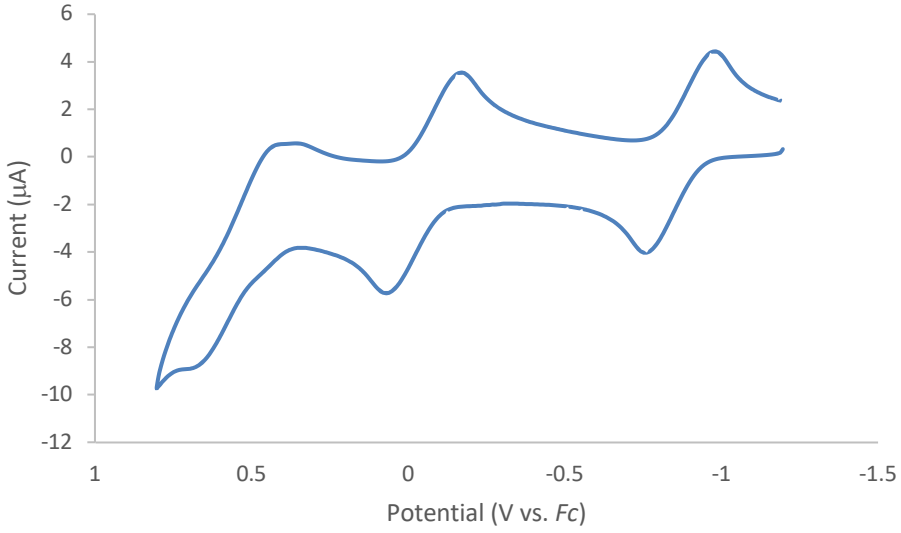

Figure 10. Cyclic voltammogram of 6. Measurements were performed on a 1 mM solution of **6** in a 50:50 mixture of toluene and THF with 0.1 M of $(n\text{-Bu})_4NPF_6$ as the electrolyte with a scan rate of 0.1 V s^{-1}. The potentials were referenced against ferrocenium (*Fc*).

To better understand the electronic and redox properties of complex **6**, we conducted a CV study. CV measurements were performed on a 1 mM solution of **6** in a 50:50 mixture of toluene and THF with 0.1 M $(n\text{-Bu})_4NPF_6$ as the electrolyte. The voltammogram of **6** is suggestive of three redox events (Figure 10). The redox potentials ($E_{1/2}$) for complex **6** are –0.87 V, –0.05 V, and –0.58 V versus *Fc*. Based on previous work from our lab, the redox events were assigned as one metal-centered redox event ($Ru^{II/III}$) and two ligand-centered redox events ($L^{-/\bullet+}$ and $L^{\bullet+/2\bullet+}$, where L = $Cz^{tBu}(Pyr^H)_2$).[80] From the CV, the $Ru^{II/III}$ and $L^{-/\bullet+}$ are reversible while the second ligand-based redox event, $L^{\bullet+/2\bullet+}$, appears to be irreversible. These values deviate slightly from analogous homoleptic complexes our group has reported based on $(Cz^{tBu}(Pyr^H)_2)_2M$ (M = Fe, Co, Ni, and Zn) (Table 3).

	$E_{1/2}$ (M^{II}/M^{III})	$E_{1/2}$ ($L^{-/\bullet+}$)	$E_{1/2}$ ($L^{\bullet+/2\bullet+}$)
6	–0.87	–0.05	0.58
$(Cz^{tBu}(Pyr^H)_2)_2Fe$	–0.64	0.61	0.85
$(Cz^{tBu}(Pyr^H)_2)_2Co$	–0.58	0.73	0.85
$(Cz^{tBu}(Pyr^H)_2)_2Ni$	n/a	0.22	0.35
$(Cz^{tBu}(Pyr^H)_2)_2Zn$	n/a	0.13	0.31

Table 3. Redox potentials (V vs. *Fc*) of 6 as compared with analogous homoleptic compounds. The redox potentials for $(Cz^{tBu}(Pyr^H)_2)_2M$ (M = Fe, Co, Ni, and Zn) were obtained from previous work.[80]

From Table 3, the redox potential for Ru^{II}/Ru^{III} is in line with other values that we have reported. For the second redox event, $L^{-/\bullet+}$, the potential for **6** more closely resembles $(Cz^{tBu}(Pyr^H)_2)_2Ni$ and $(Cz^{tBu}(Pyr^H)_2)_2Zn$ than the Fe or Co complexes, likely due to the number

of unpaired electrons. For the third redox event, $L^{\bullet+/2\bullet+}$, the potential for **6** appears to agree with other complexes of this type.

Comparing the potential for the $Ru^{II/III}$ redox couple of **6** to those of other Ru(II) complexes in the polypyridyl family, the $E_{1/2}$ we measure differs. The single electron oxidation from Ru^{II} to Ru^{III} for $[Ru(bpy)_3]^{2+}$ was reported to be 0.88 V (vs. *Fc*).[89] Further, the $Ru^{II/III}$ redox couple for $[Ru(phen)_3]^{2+}$ was measured at 0.90 V (vs. *Fc*).[89] The value we record for the $Ru^{II/III}$ redox couple of **6** occurs at negative potentials, which implies **6** is easier to be oxidized. This is in contrast to positive potentials for the $Ru^{II/III}$ redox couple reported for established Ru(II) systems.[89] The potential for the metal-based redox event we record for **6** is more in line with our analogous homoleptic compounds. This difference may be due to the redox properties of our tridentate N,N,N-ligand system differing from polypyridyl ligands.

Given the potential for **6** to access multiple redox states as demonstrated by CV, we wanted to examine these oxidized intermediates to see if they can be isolated. To this end, we hoped to perform a series of chemical oxidations on **6** using varying equivalences of oxidant. We conducted a small pilot reaction as a proof of concept. Upon the treatment of **6** with 1 equivalent of ferrocenium hexafluorophosphate ($FcPF_6$) in toluene, the red solution of **6** immediately took on a green color. The resulting slurry was allowed to react overnight. The product was isolated by filtering through a Celite plug and collected using MeCN. Though this product has yet to be fully characterized, the results are promising. The ^1H NMR spectrum of $\mathbf{6}^+$ shows paramagnetically shifted resonances (Figure 14). This suggests that the Ru(II) center underwent oxidation, likely to Ru(III) upon treating **6** with one equivalent of oxidant. Attempts to isolate and characterize $\mathbf{6}^+$ along with its more oxidized counterparts are currently ongoing.

Concluding Remarks for Complex 6

We have successfully synthesized a homoleptic complex supported by a Ru(II) center using $HCz^{tBu}(Pyr^{H})_2$. Unfortunately, attempts to synthesize a homoleptic complex using $HCz^{tBu}(Pyr^{Me})_2$ and $HCz^{tBu}(Pyr^{iPr})_2$ were not yet fruitful. We elaborate on why $HCz^{tBu}(Pyr^{Me})_2$ and $HCz^{tBu}(Pyr^{iPr})_2$ were not successful in Chapter IV. Overall, complex **6** was characterized using ^{1}H NMR spectroscopy, X-ray crystallography, UV-Vis spectroscopy, and CV. Preliminary results for this complex are promising. Though CV measurements for the $Ru^{II/III}$ redox couple differ from established Ru(II) systems, the strong absorbance band elucidated via UV-Vis for **6** is in line with previously reported Ru(II) polypyridyl complexes that function as PS. Given these encouraging characteristics, complex **6** merits further investigation.

Synthesis and Characterization of Complex 7

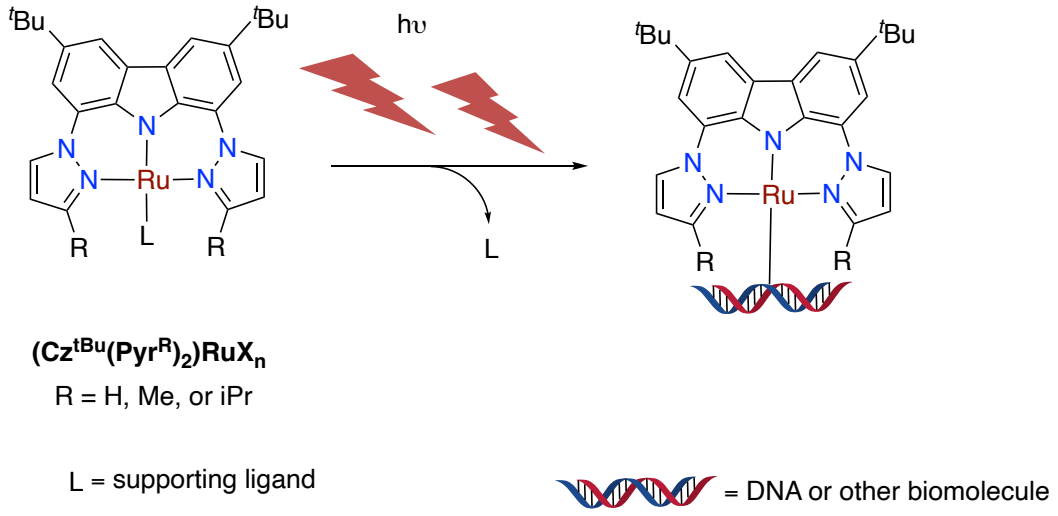

Scheme 4. Photoinduced ligand dissociation. Ligand dissociation envisioned with our tridentate ligand.

Having produced and characterized the homoleptic complex **6**, we wanted to generate a compound that is analogous to **6**, but is coordinated to one less $Cz^{tBu}(Pyr^{H})_2^-$ ligand. We envisioned a complex of the type $Cz^{tBu}(Pyr^{R})_2RuX_n$ (where X_n = supporting ligands) (Scheme 4).

Our goal of synthesizing a Ru(II) complex of this type is so that this complex can have an open coordination site upon the dissociation of more labile supporting ligands. This rational is based on the precedent of other drug candidates. NAMI-A, KP1091, and KP1339, which are presented in Figure 2, are examples of Ru complexes that feature labile chloro ligands. It is important to point out that these compounds do not function as PS. Rather, upon the dissociation of the labile chloro ligands these complexes can bind to DNA. Additionally, there are examples of Ru compounds where ligand dissociation is photoinduced.[90] This system may have applications in medicine.[90] Scheme 4 shows a potential mechanism of this using our ligand system. Though, this is beyond the scope of this work, it could be an avenue of further inquiry in the future. With this approach in mind, we set out to produce a compound that is structurally similar to **6** but has one less NNN-pincer ligand.

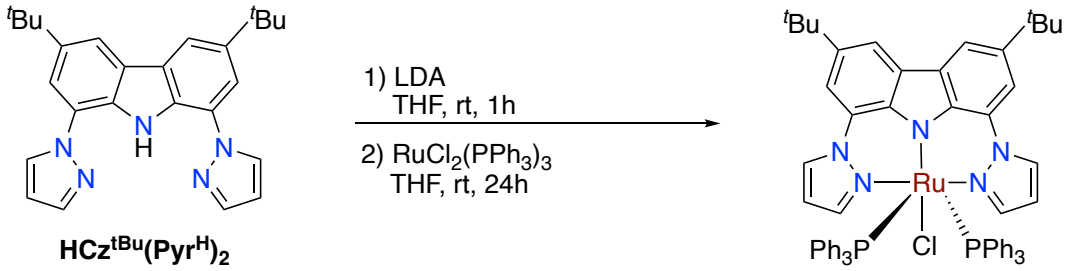

HCz^{tBu}(Pyr^{H})$_2$ **1** **7**

Scheme 5. Synthesis of complex 7.

Herein, we report the synthesis of complex **7** (Scheme 5). Complex **7** was prepared using a similar method through which **6** was synthesized. HCz^{tBu}(Pyr^{H})$_2$ was treated with one equivalence of LDA to deprotonate the carbazole nitrogen. Next, transmetalation was performed by adding the deprotonated ligand to one equivalence of $RuCl_2(PPh_3)_3$ in THF at ambient temperature and under inert N_2 atmosphere (Scheme 5). Similar to what is reported for **6**, ^{1}H NMR spectroscopy of **7** shows diamagnetic resonances which are in agreement with a d^6 low-

spin Ru(II) center (Figure 15).

Crystal Structure of 7

Red crystals of **7** were grown for X-ray crystallography from a concentrated solution of toluene. The crystal structure of **7** was solved (Figure 11). The solid-state structure of **7** was found to be a heteroleptic complex whereby the Ru center is supported by one molecule of $Cz^{tBu}(Pyr^{H})_2^-$, two molecules of triphenylphosphine (PPh_3), and one Cl^- ion. The bond angle between N_{CZ} (N3), Ru (Ru1), and Cl (Cl1) was found to be 175°. This suggest that the geometry of **7** is best characterized as a distorted octahedral geometry due to slight deviation from an ideal octahedral geometry of 180°. Complex **7** is slightly more distorted than **6**, with bond angles measuring 175° and 179°, respectively.

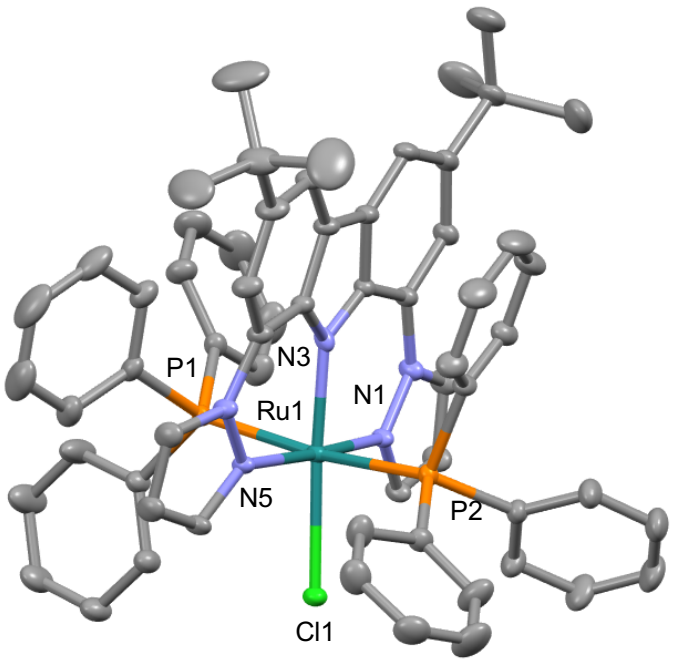

Figure 11. Molecular structure of complex 7.

Selected bond lengths for complex **7** are reported (Table 4). The distance from the N_{Pyr} to Ru (Ru1) was found to be 2.093(2) Å for N1 and 2.077(2) Å for N5. The bond lengths from the

N_{Pyr} to the Ru center are elongated by ~0.05–0.70 Å for complex **7** compared to **6**. The bond distance from N_{CZ} (N3) to Ru (Ru1) was found to be 2.017(2) Å. This value is nearly identical to the corresponding N_{CZ}–Ru bonds distance reported for **6**, differing by only 0.005 Å. The Ru–N bond in $[Ru(bpy)_3]^{2+}$ was reported as 2.057(3) Å.[81] This distance is ~0.04 Å longer than the N_{CZ}–Ru bond distance and only slightly longer than the N_{Pyr}–Ru bond distances. Further corroborating these results, the N–Ru bond lengths we report for **7** are similar to those of $[Ru(phen)_2(bpy)]^{2+}$.[82,83]

Number	Object 1	Object 2	Length (Å)
1	N3	Ru1	2.017(2)
2	Cl1	Ru1	2.4953(7)
3	N1	Ru1	2.093(2)
4	P1	Ru1	2.4010(5)
5	P2	Ru1	2.4439(5)
6	Ru1	N5	2.077(2)

Table 4. Selected bond distances for 7. Bond lengths are reported in angstroms (Å).

The bond distance from P(P1) to Ru(R1) and P2 to R (Ru1) was 2.4010(5) and 2.4439(5) Å, respectively. These values may be a reflection of the distorted geometry of 7. The average Ru–P bond length for complex **7** is 2.4225(5) Å. The Ru–P bond length of **7** is in line with other examples that have been reported in the literature. For example, Zeng and Yu report a series of N,N,N-complex bearing a PPh_3 ligand.[91] In their complexes, they find the Ru–P bonds to be 2.367(6), 2.369(13), and 2.347(18) Å.[91] These values are similar to the Ru–P bond length observed in **7**, though the values they report are slightly shorter. Betley and coworkers have also

reported a series of N,N,N-complexes that feature a Ru center and PPh_3 ligands.[92] In their system the Ru–P bond distances were 2.397(1) and 2.378(1) Å.[92] These bond distances are similar to our results and demonstrates the Ru–P distance in **7** are consistent with values in the literature.

UV-Visible Spectrum of 7

Absorption measurements were performed on a 1 mM solution of **7** in MeCN (Figure 12). The UV-Vis absorption spectrum of **7** reveals a longest wavelength absorption maxima at 478 nm. This value is more red-shifted compared to the 432 nm observed for complex **6**. In addition, this absorption band is consistent with ^{1}LC and ^{1}MLCT transitions.[64,65] The absorption maxima at 478 nm for **7** is in line with other Ru(II) polypyridyl complexes, like $[Ru(bpy)_3]^{2+}$ and TLD1433. For example, $[Ru(bpy)_3]^{2+}$ was reported to have an absorption maxima at 450 nm.[84–87] TLD1433, on the other hand, had a longest wavelength absorption maxima at 420 nm.[88] These values are in agreement with the wavelength we reported for complex **7** and in assigning this absorption band as ^{1}LC and ^{1}MLCT transitions.

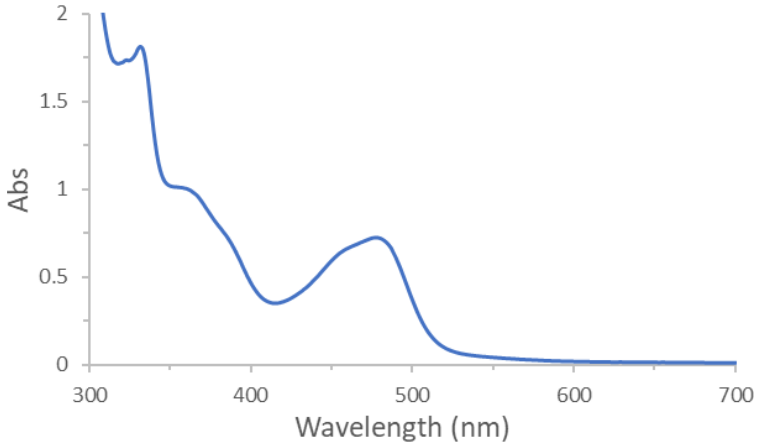

Figure 12. Absorption spectrum of 7. Absorption measurements are based on a 1 mM solution of **7** in MeCN.

Concluding Remarks for Complex 7

Within, we describe the synthesis of a heteroleptic complex **7** using $HCz^{tBu}(Pyr^H)_2$. This

system was characterized using ^{1}H NMR spectroscopy, X-ray crystallography, and UV-Vis. Attempts to synthesize an analogous form of **7** using $HCz^{tBu}(Pyr^{Me})_2$ and $HCz^{tBu}(Pyr^{iPr})_2$ were not successful. Unfortunately, we were not able to further characterize **7** due to a limited supply of product on hand. This is because the synthesis of **7** was not reproducible. Further attempts to synthesize a heteroleptic complex using an alternative Ru(II) salt, [Ru(*p*-cymene)Cl_2]$_2$ were also unsuccessful. Inspired by the Ru(II) polypyridyl family of complexes, we tried to react **7** with 1,10- phenanthroline. We hypothesized this would cause two supporting ligands from **7** to dissociate, leading to the coordination of 1,10-phenanthroline to the metal center. We heated a solution of **7** with one equivalent of 1,10 phenanthroline in THF at 70 °C overnight in a bomb flask using a modified synthetic procedure.[88] Unfortunately, this reaction was not successful.

CHAPTER IV

DISCUSSION AND FUTURE WORK

Herein, the work that was introduced in this thesis will be discussed. We will also describe potential synthetic challenges we encountered and why they may have occurred. Finally, we will introduce currently ongoing and future experiments to complement this work. Overall, the goal of this thesis was to determine whether our established carbazole-based N,N,N-pincer ligand platform, $Cz^{tBu}(Pyr^{R})_2$ (R = H, Me, iPr), can be used to support Ru(II) complexes. To this end, we have described the synthesis of two novel Ru compounds, **6** and **7**.

Initial effort in this endeavor began by generating a homoleptic complex based on the $Cz^{tBu}(Pyr^{R})_2^-$ (R = H, Me, iPr) ligand platform. Of these N,N,N-pincer ligands, only $Cz^{tBu}(Pyr^{H})_2^-$ was found to be capable of supporting a Ru(II) center. The resulting compound **6** is a homoleptic complex, where Ru(II) is coordinated by two molecules of $Cz^{tBu}(Pyr^{H})_2^-$. One possible reason why $Cz^{tBu}(Pyr^{Me})_2^-$ or $Cz^{tBu}(Pyr^{iPr})_2^-$ were not successful in supporting Ru(II) homoleptic complex could be due to the more sterically encumbered pyrazole arms. This higher steric effect may result in formation of the homoleptic complex based on $Cz^{tBu}(Pyr^{Me})_2^-$ or $Cz^{tBu}(Pyr^{iPr})_2^-$ not being energetically favorable. Our group has had success in generating Fe, Co, Ni, and Zn homoleptic complexes supported by more sterically encumbered ligands like $Cz^{tBu}(Pyr^{iPr})_2^-$.[80] A manuscript with these results is being prepared for publication. Thus, it is unlikely using more sterically bulky ligands made the formation of homoleptic complexes less favorable. One other possibility is the production of homoleptic complexes with $Cz^{tBu}(Pyr^{Me})_2^-$ or $Cz^{tBu}(Pyr^{iPr})_2^-$ may not be

favorable when using 4d transition metals, such as Ru.

One of the most encouraging pieces of data collected for **6** is its absorption spectrum. The absorption spectrum of **6** reveals a ^{1}MLCT transition with maxima at 432 nm. Interestingly, this absorption band tails to ~650 nm. This feature is promising since the absorption band of **6**, especially when considering the latter portion, is more red-shifted than complexes in the Ru(II) polypyridyl family. This is important because the absorption band of **6** is broader. Thus, it falls more in the range of the ideal PDT window of ~600–900 nm.[90] Complexes that have absorption values in this range can be activated using longer wavelengths of light, which penetrate tissue deeper than shorter wavelengths.[90,93,94]

In the future, we want to gather more photophysical data on complex **6**. Specifically, we hope to find a collaborator who can assist in measuring the excited-state life time of **6**, as well as testing whether **6** can produce $^1O_2$ to assess its potential as a PS for PDT. Further, we plan to continue studying the redox properties of **6** and attempt to isolate more oxidized intermediates.

We also described the synthesis of complex **7** and characterized it using ^{1}H NMR spectroscopy, X-ray crystallography, and UV-Vis spectroscopy. One rather disappointing part of this work has been that the reaction to form **7** was not reproducible. This hindered the amount of data that we were able to gather on **7** because of a limited supply of product. In the future, we hope to overcome this synthetic challenge by optimizing the reaction conditions to see if a heteroleptic complex can be formed.

Despite this drawback, the data we were able to collect on **7** paint a picture that is in line with other examples of Ru(II) complexes. In particular, the absorption spectrum of **7** shows a ^{1}MLCT transition at 478 nm. This absorption maxima is red-shifted by ~50 nm compared to **6**. One possible explanation for this is the increased delocalized electrons that **7** has due to the PPh_3

ligands. Further, we found that the geometry of **7** was slightly more distorted than **6**. This may be due to **7** taking on a more distorted octahedral geometry as a result of the steric bulkiness of the PPh_3 ligands.

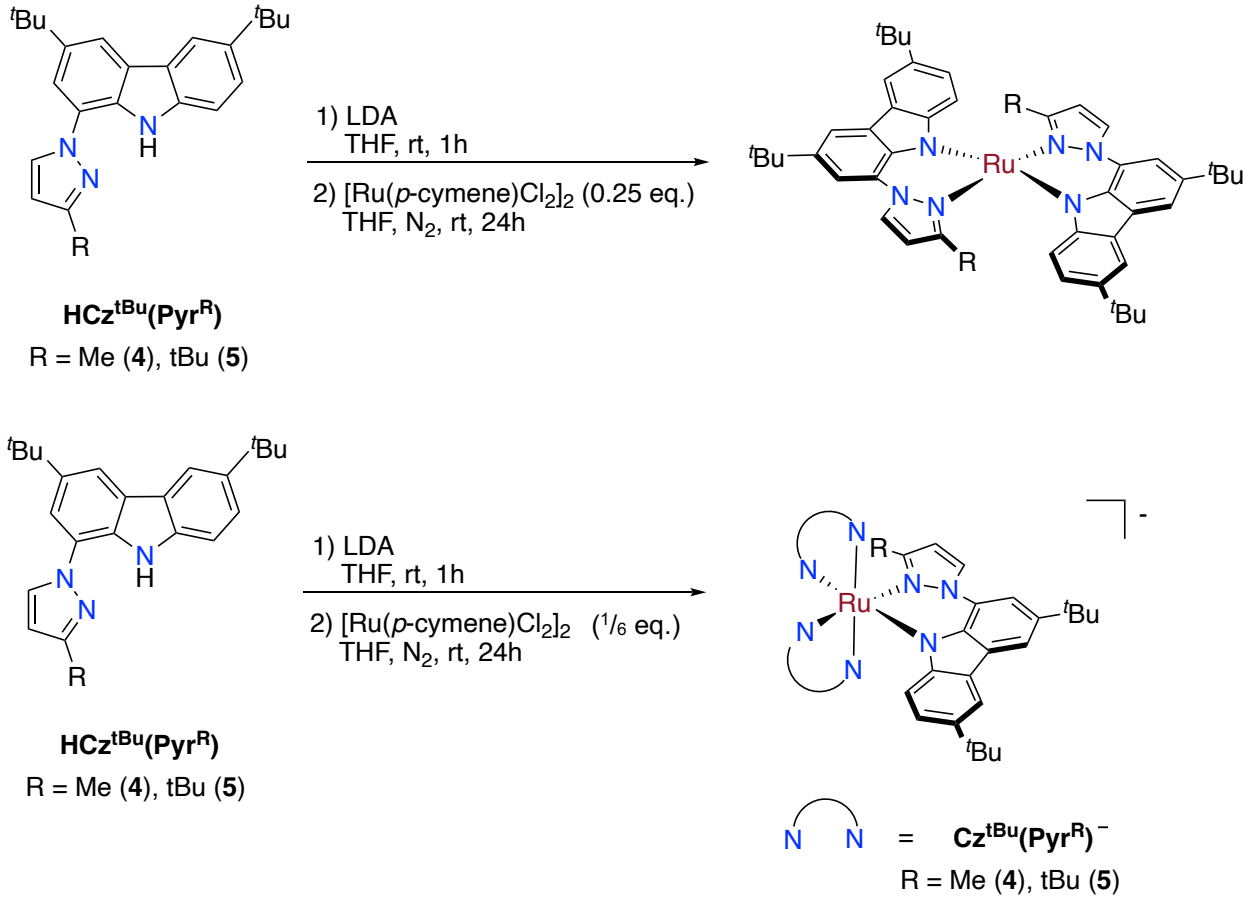

Scheme 6. Proposed synthesis of four- and six-coordinate complexes.

Lastly, current work on this project has focused on synthesizing a heteroleptic or homoleptic complex using the N,N-bidentate ligands, $Cz^{tBu}(Pyr^{Me})^-$ or $Cz^{tBu}(Pyr^{tBu})^-$. Attempts to synthesize a Ru(II) complexes supported by these bidentate ligand systems are currently ongoing. Given that $Cz^{tBu}(Pyr^{Me})^-$ and $Cz^{tBu}(Pyr^{tBu})^-$ are bidentate ligands, we predict that they will be able to form four-coordinate or six-coordinate complexes with Ru(II) (Scheme 6). In addition, we hope to contribute to the Ru(II) polypyridyl family of complexes by proposing the

synthesis of a novel Ru system supported by $Cz^{tBu}(Pyr^{Me})^-$ or $Cz^{tBu}(Pyr^{tBu})^-$ and two bipyridine ligands (Scheme 7). This proposed synthesis is based on a modified reaction from the literature.[88,95]

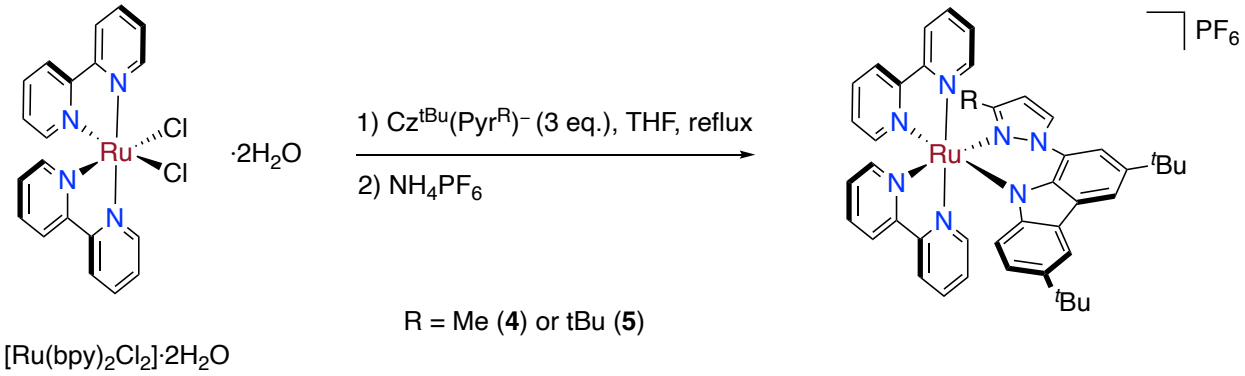

Scheme 7. Proposed synthesis of a ruthenium(II) polypyridyl complex based on our N,N-ligand.

Overall, this work has demonstrated that our established tridentate N,N,N-pincer ligand system can be used to support a homoleptic and heteroleptic complex with Ru(II). Future research goals include examining the photophysical properties of these compounds more in depth and overcoming the synthetic challenges that were described. Additionally, further studies should investigate the redox properties of these compounds, particularly the redox chemistry of the homoleptic complex **6**. Indeed, this work further shows the versatility of our ligand system in supporting a variety of metal complexes beyond first-row transition metals. We hope that this work and the results presented herein will contribute to the body of PDT research on Ru complexes that has already been conducted. We are optimistic on the future direction of this project.

APPENDIX A

SUPPLEMENTARY INFORMATION

^{1}H NMR Spectroscopy

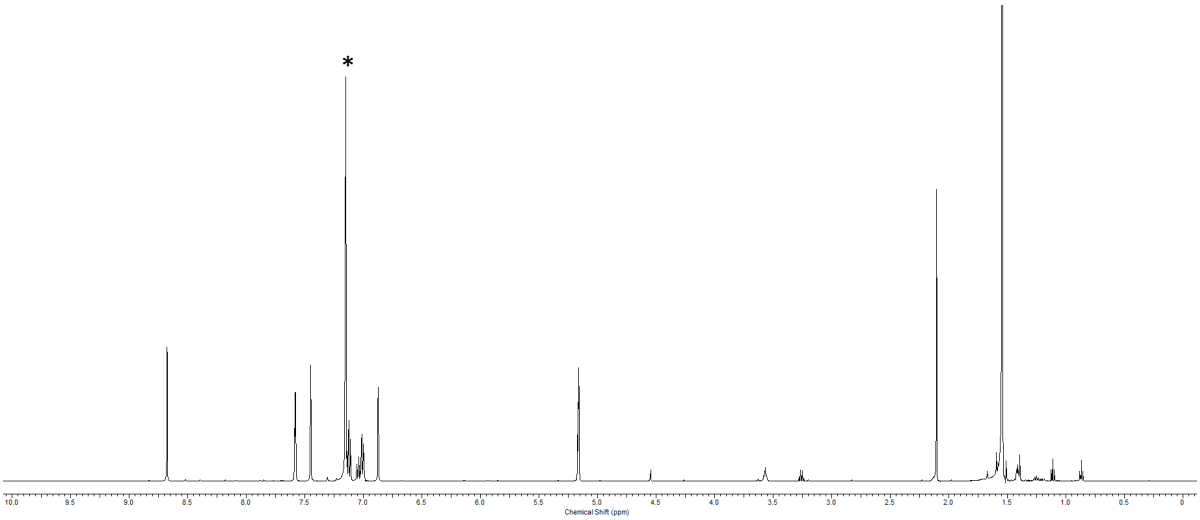

Figure 13. ^{1}H NMR of 6 in C_6D_6. Residual solvent(s) indicated by: *

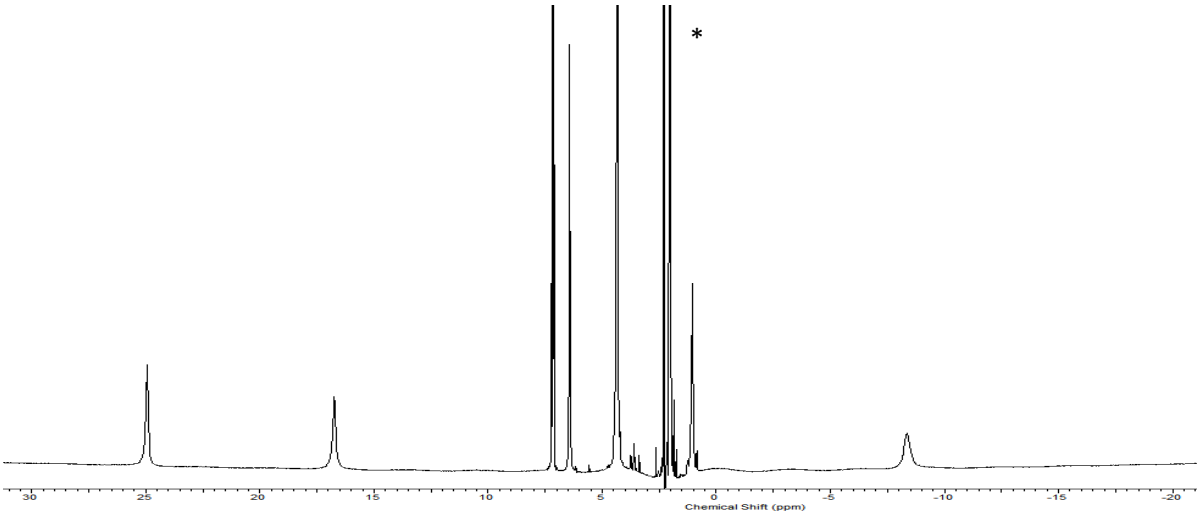

Figure 14. ^{1}H NMR of 6^{+} in acetone-d_6. Residual solvent(s) indicated by: *

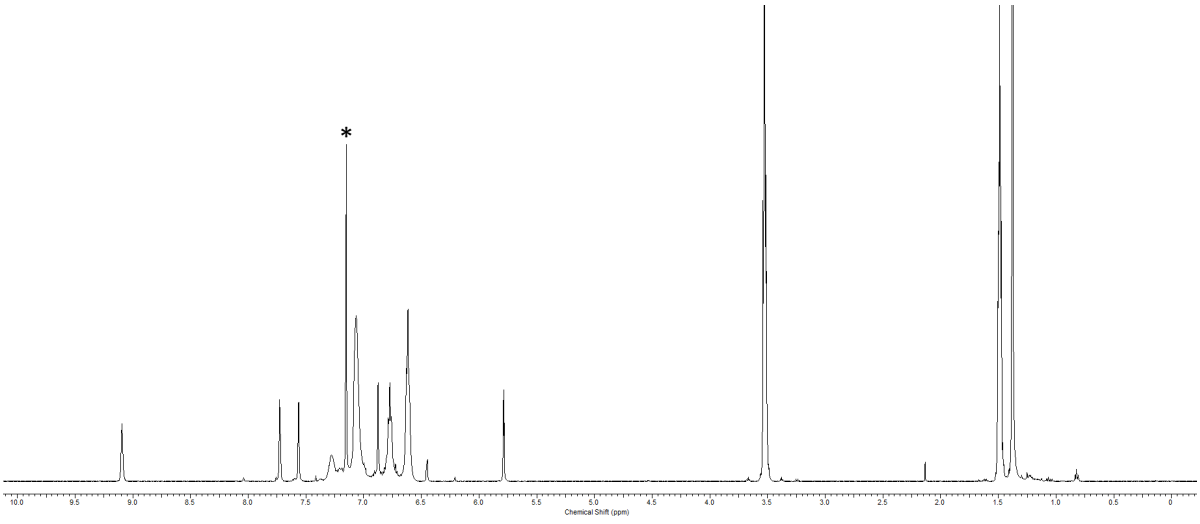

Figure 15. ^{1}H NMR of 7 in C_6D_6. Residual solvent(s) indicated by: *

Crystallographic parameters

For complex **6**, the structure was solved using the parameters discussed herein. Four of eight *tert*-butyl groups are disordered by rotation. The disordered moieties were restrained to have similar geometries as another not disordered *tert*-butyl group. Uji components of ADPs for disordered atoms closer to each other than 2.0 Angstrom were restrained to be similar. Subject to these conditions the occupancy rations refined to 0.912(3) to 0.088(3) (group of C7), 0.614(4) to 0.386(4) (C44), 0.702(4) to 0.298(4) (C70) and 0.829(4) to 0.171(4) (C97).

A toluene solvate molecule was refined as disordered by a slight shift. The two disordered moieties were restrained to have similar geometries. Uji components of ADPs for disordered atoms closer to each other than 2.0 Angstroms were restrained to be similar. Subject to these conditions the occupancy ratio was refined to 0.608(7) to 0.392(7).

The structure contains additional 1557 Ang3 of solvent accessible voids. Part of the residual electron density peaks indicate the presence of additional highly disordered toluene as well as other ill-defined solvate molecules. No meaningful, self-consistent model could be

developed for the content of these voids. The structure factors were instead augmented via reverse Fourier transforms methods using the SQUEEZE routine as implemented in the program Platon.[96] The resulting FAB file containing the structure factor contribution from the electron content of the void space was used in together with the original hkl file in the further refinement. The SQUEEZE procedure corrected for 396 electrons within the solvent accessible voids.

For complex **7**, the structure was solved using the crystallographic parameters. One of two *tert*-butyl groups is disordered by rotation. The two disordered moieties were restrained to have similar geometries as the other not disordered *tert*-butyl group. Uji components of ADPs for disordered atoms closer to each other than 2.0 Angstroms were restrained to be similar. Subject to these conditions the occupancy ratio refined to 0.630(15) to 0.370(15).

Two of three solvate toluene molecules were refined as disordered by slight rotations. The two disordered moieties were restrained to have similar geometries as the third not disordered toluene molecule. Uji components of ADPs for disordered atoms closer to each other than 2.0 Angstroms were restrained to be similar. Subject to these conditions the occupancy ratio refined to 0.552(6) to 0.448(6) for the toluene of C71, and to 0.618(8) to 0.372(8) for the toluene of C78.

	6	**7**·3(C_7H_8)
Chemical formula	$C_{20}H_{20}N_6Ru$	$C_{62}H_{58}ClN_5P_2Ru$
M_r	445.49	1347.99
Crystal system, space group	Triclinic, *P*1	Triclinic, *P*1
Temperature (K)	150	150
a (Å) *b* (Å) *c* (Å)	18.4921 (11) 18.6394 (12) 23.2059 (14)	14.7296 (6) 15.0156 (7) 17.3071 (8)
α (°) β (°) γ (°)	87.947 (3) 66.808 (2) 61.087 (2)	107.650 (2) 105.496 (2) 97.467 (2)
V (Å^3)	6316.0 (7)	3421.1 (3)
Z	12	2
Radiation type	Mo *K*α	Mo *K*α
μ (mm^{-1})	0.76	0.37
Crystal size (mm)	n/a	0.49 × 0.45 × 0.33
T_{min}, T_{max}	n/a	0.682, 0.747
[$I > 2\sigma(I)$] reflections	104463, 46016, 29160	188125, 26151, 20889
R_{int}	0.041	0.048
$(\sin\theta/\lambda)_{max}$ (Å^{-1})	0.770	0.771
$R[F^2 > 2\sigma(F^2)]$, $wR(F^2)$, S	0.057, 0.194, 0.98	0.049, 0.113, 1.09
No. of reflections	46061	26151
No. of parameters	1710	1008
No. of restraints	1359	1842
H-atom treatment	H-atom parameters constrained	H-atom parameters constrained
$\Delta\rho_{max}$, $\Delta\rho_{min}$ (e Å^{-3})	1.68, −1.49 ($(\Delta/\sigma)_{max}$ = 1.890))	1.31, −0.94

Table 5. Crystallographic parameters for 6 and 7. The crystal of **6** was refined using the *SHELXL* program.[97] The crystal of **7** was refined using the following program suite: *SHELXL*,[97] *SHELXL* Rev1231,[98] *SHELXL2018/3*,[99] Apex3 v2019.1,[100] *SAINT* V8.40B.[101]

REFERENCE LIST

(1) Ahmad, F. B.; Cisewski, J. A.; Miniño, A.; Anderson, R. N. Provisional Mortality Data — United States, 2020. *MMWR Morb. Mortal. Wkly. Rep.* **2021**, *70* (14), 519–522. https://doi.org/10.15585/mmwr.mm7014e1.

(2) Ahmad, F. B.; Anderson, R. N. The Leading Causes of Death in the US for 2020. *JAMA* **2021**, *325* (18), 1829. https://doi.org/10.1001/jama.2021.5469.

(3) Types of Cancer Treatment - National Cancer Institute https://www.cancer.gov/about-cancer/treatment/types (accessed 2022 -01 -08).

(4) Mullard, A. 2020 FDA Drug Approvals. *Nat. Rev. Drug Discov.* **2021**, *20* (2), 85–90. https://doi.org/10.1038/d41573-021-00002-0.

(5) Mansoori, B.; Mohammadi, A.; Davudian, S.; Shirjang, S.; Baradaran, B. The Different Mechanisms of Cancer Drug Resistance: A Brief Review. *Adv. Pharm. Bull.* **2017**, *7* (3), 339–348. https://doi.org/10.15171/apb.2017.041.

(6) Housman, G.; Byler, S.; Heerboth, S.; Lapinska, K.; Longacre, M.; Snyder, N.; Sarkar, S. Drug Resistance in Cancer: An Overview. *Cancers* **2014**, *6* (3), 1769–1792. https://doi.org/10.3390/cancers6031769.

(7) Monro, S.; Colón, K. L.; Yin, H.; Roque, J.; Konda, P.; Gujar, S.; Thummel, R. P.; Lilge, L.; Cameron, C. G.; McFarland, S. A. Transition Metal Complexes and Photodynamic Therapy from a Tumor-Centered Approach: Challenges, Opportunities, and Highlights from the Development of TLD1433. *Chem. Rev.* **2019**, *119* (2), 797–828. https://doi.org/10.1021/acs.chemrev.8b00211.

(8) Mjos, K. D.; Orvig, C. Metallodrugs in Medicinal Inorganic Chemistry. *Chem. Rev.* **2014**, *114* (8), 4540–4563. https://doi.org/10.1021/cr400460s.

(9) Johnstone, T. C.; Park, G. Y.; Lippard, S. J. Understanding and Improving Platinum Anticancer Drugs--Phenanthriplatin. *Anticancer Res.* **2014**, *34* (1), 471–476.

(10) Apps, M. G.; Choi, E. H. Y.; Wheate, N. J. The State-of-Play and Future of Platinum Drugs. *Endocr. Relat. Cancer* **2015**, *22* (4), R219–R233. https://doi.org/10.1530/ERC-15-0237.

(11) Dasari, S.; Tchounwou, P. B. Cisplatin in Cancer Therapy: Molecular Mechanisms of Action. *Eur. J. Pharmacol.* **2014**, *740*, 364–378. https://doi.org/10.1016/j.ejphar.2014.07.025.

(12) Zhang, Q.; Lu, Q.-B. New Combination Chemotherapy of Cisplatin with an Electron-Donating Compound for Treatment of Multiple Cancers. *Sci. Rep.* **2021**, *11* (1), 788. https://doi.org/10.1038/s41598-020-80876-z.

(13) Rose, P. G.; Bundy, B. N.; Watkins, E. B.; Thigpen, J. T.; Deppe, G.; Maiman, M. A.; Clarke-Pearson, D. L.; Insalaco, S. Concurrent Cisplatin-Based Radiotherapy and Chemotherapy for Locally Advanced Cervical Cancer. *N. Engl. J. Med.* **1999**, *340* (15), 1144–1153. https://doi.org/10.1056/NEJM199904153401502.

(14) Fuertes, M. A.; Alonso, C.; Pérez, J. M. Biochemical Modulation of Cisplatin Mechanisms of Action: Enhancement of Antitumor Activity and Circumvention of Drug Resistance. *Chem. Rev.* **2003**, *103* (3), 645–662. https://doi.org/10.1021/cr020010d.

(15) Oun, R.; Moussa, Y. E.; Wheate, N. J. The Side Effects of Platinum-Based Chemotherapy Drugs: A Review for Chemists. *Dalton Trans.* **2018**, *47* (19), 6645–6653. https://doi.org/10.1039/C8DT00838H.

(16) Johnstone, T. C.; Suntharalingam, K.; Lippard, S. J. Third Row Transition Metals for the Treatment of Cancer. *Philos. Transact. A Math. Phys. Eng. Sci.* **2015**, *373* (2037), 20140185. https://doi.org/10.1098/rsta.2014.0185.

(17) Howell, S. B.; Safaei, R.; Larson, C. A.; Sailor, M. J. Copper Transporters and the Cellular Pharmacology of the Platinum-Containing Cancer Drugs. *Mol. Pharmacol.* **2010**, *77* (6), 887–894. https://doi.org/10.1124/mol.109.063172.

(18) Johnstone, T. C.; Suntharalingam, K.; Lippard, S. J. The Next Generation of Platinum Drugs: Targeted Pt(II) Agents, Nanoparticle Delivery, and Pt(IV) Prodrugs. *Chem. Rev.* **2016**, *116* (5), 3436–3486. https://doi.org/10.1021/acs.chemrev.5b00597.

(19) Culy, C. R.; Clemett, D.; Wiseman, L. R. Oxaliplatin. A Review of Its Pharmacological Properties and Clinical Efficacy in Metastatic Colorectal Cancer and Its Potential in Other Malignancies. *Drugs* **2000**, *60* (4), 895–924. https://doi.org/10.2165/00003495-200060040-00005.

(20) Bergamo, A.; Sava, G. Ruthenium Anticancer Compounds: Myths and Realities of the Emerging Metal-Based Drugs. *Dalton Trans.* **2011**, *40* (31), 7817–7823. https://doi.org/10.1039/C0DT01816C.

(21) Bergamo, A.; Messori, L.; Piccioli, F.; Cocchietto, M.; Sava, G. Biological Role of Adduct Formation of the Ruthenium(III) Complex NAMI-A with Serum Albumin and Serum Transferrin. *Invest. New Drugs* **2003**, *21* (4), 401–411. https://doi.org/10.1023/a:1026243000320.

(22) Alessio, E.; Mestroni, G.; Bergamo, A.; Sava, G. Ruthenium Antimetastatic Agents. *Curr. Top. Med. Chem. 4* (15), 1525–1535.

(23) Lin, K.; Zhao, Z.-Z.; Bo, H.-B.; Hao, X.-J.; Wang, J.-Q. Applications of Ruthenium Complex in Tumor Diagnosis and Therapy. *Front. Pharmacol.* **2018**, *9*.

(24) Bergamo, A.; Riedel, T.; Dyson, P. J.; Sava, G. Preclinical Combination Therapy of the Investigational Drug NAMI-A(+) with Doxorubicin for Mammary Cancer. *Invest. New Drugs* **2015**, *33* (1), 53–63. https://doi.org/10.1007/s10637-014-0175-5.

(25) Hartinger, C. G.; Zorbas-Seifried, S.; Jakupec, M. A.; Kynast, B.; Zorbas, H.; Keppler, B. K. From Bench to Bedside – Preclinical and Early Clinical Development of the Anticancer Agent Indazolium Trans-[Tetrachlorobis(1H-Indazole)Ruthenate(III)] (KP1019 or FFC14A). *J. Inorg. Biochem.* **2006**, *100* (5), 891–904. https://doi.org/10.1016/j.jinorgbio.2006.02.013.

(26) Hartinger, C. G.; Jakupec, M. A.; Zorbas-Seifried, S.; Groessl, M.; Egger, A.; Berger, W.; Zorbas, H.; Dyson, P. J.; Keppler, B. K. KP1019, A New Redox-Active Anticancer Agent – Preclinical Development and Results of a Clinical Phase I Study in Tumor Patients. *Chem. Biodivers.* **2008**, *5* (10), 2140–2155. https://doi.org/10.1002/cbdv.200890195.

(27) Heffeter, P.; Böck, K.; Atil, B.; Reza Hoda, M. A.; Körner, W.; Bartel, C.; Jungwirth, U.; Keppler, B. K.; Micksche, M.; Berger, W.; Koellensperger, G. Intracellular Protein Binding Patterns of the Anticancer Ruthenium Drugs KP1019 and KP1339. *J. Biol. Inorg. Chem. JBIC Publ. Soc. Biol. Inorg. Chem.* **2010**, *15* (5), 737–748. https://doi.org/10.1007/s00775-010-0642-1.

(28) Mari, C.; Pierroz, V.; Ferrari, S.; Gilles Gasser. Combination of Ru(II) Complexes and Light: New Frontiers in Cancer Therapy. *Chem. Sci.* **2015**, *6* (5), 2660–2686. https://doi.org/10.1039/C4SC03759F.

(29) Kurzwernhart, A.; Kandioller, W.; Bartel, C.; Bächler, S.; Trondl, R.; Mühlgassner, G.; Jakupec, M. A.; Arion, V. B.; Marko, D.; Keppler, B. K.; Hartinger, C. G. Targeting the DNA-Topoisomerase Complex in a Double-Strike Approach with a Topoisomerase Inhibiting Moiety and Covalent DNA Binder. *Chem. Commun.* **2012**, *48* (40), 4839–4841. https://doi.org/10.1039/C2CC31040F.

(30) Kou, J.-F.; Qian, C.; Wang, J.-Q.; Chen, X.; Wang, L.-L.; Chao, H.; Ji, L.-N. Chiral Ruthenium(II) Anthraquinone Complexes as Dual Inhibitors of Topoisomerases I and II. *J. Biol. Inorg. Chem. JBIC Publ. Soc. Biol. Inorg. Chem.* **2012**, *17* (1), 81–96. https://doi.org/10.1007/s00775-011-0831-6.

(31) Wang, J.-Q.; Zhao, Z.-Z.; Bo, H.-B.; Chen, Q.-Z. Synthesis, Characterization, and Antitumor Properties of Ruthenium(II) Anthraquinone Complexes. *J. Coord. Chem.* **2016**, *69* (2), 177–189. https://doi.org/10.1080/00958972.2015.1120291.

(32) Wang, J.-Q.; Zhang, P.-Y.; Qian, C.; Hou, X.-J.; Ji, L.-N.; Chao, H. Mitochondria Are the Primary Target in the Induction of Apoptosis by Chiral Ruthenium(II) Polypyridyl Complexes in Cancer Cells. *J. Biol. Inorg. Chem. JBIC Publ. Soc. Biol. Inorg. Chem.* **2014**, *19* (3), 335–348. https://doi.org/10.1007/s00775-013-1069-2.

(33) Liu, J.; Chen, Y.; Li, G.; Zhang, P.; Jin, C.; Zeng, L.; Ji, L.; Chao, H. Ruthenium(II) Polypyridyl Complexes as Mitochondria-Targeted Two-Photon Photodynamic Anticancer Agents. *Biomaterials* **2015**, *56*, 140–153. https://doi.org/10.1016/j.biomaterials.2015.04.002.

(34) Wan, D.; Tang, B.; Wang, Y.-J.; Guo, B.-H.; Yin, H.; Yi, Q.-Y.; Liu, Y.-J. Synthesis and Anticancer Properties of Ruthenium (II) Complexes as Potent Apoptosis Inducers through Mitochondrial Disruption. *Eur. J. Med. Chem.* **2017**, *139*, 180–190. https://doi.org/10.1016/j.ejmech.2017.07.066.

(35) Gill, M. R.; Cecchin, D.; Walker, M. G.; Mulla, R. S.; Battaglia, G.; Smythe, C.; Thomas, J. A. Targeting the Endoplasmic Reticulum with a Membrane-Interactive Luminescent Ruthenium(Ii) Polypyridyl Complex†Electronic Supplementary Information (ESI) Available: Experimental Details, Characterization of 2 and Fig. S1-S6. See DOI: 10.1039/C3sc51725jClick Here for Additional Data File. *Chem. Sci.* **2013**, *4* (12), 4512–4519. https://doi.org/10.1039/c3sc51725j.

(36) Zeng, L.; Gupta, P.; Chen, Y.; Wang, E.; Ji, L.; Chao, H.; Chen, Z.-S. The Development of Anticancer Ruthenium(II) Complexes: From Single Molecule Compounds to Nanomaterials. *Chem. Soc. Rev.* **2017**, *46* (19), 5771–5804. https://doi.org/10.1039/c7cs00195a.

(37) Rui, L.-L.; Cao, H.-L.; Xue, Y.-D.; Liu, L.-C.; Xu, L.; Gao, Y.; Zhang, W.-A. Functional Organic Nanoparticles for Photodynamic Therapy. *Chin. Chem. Lett.* **2016**, *27* (8), 1412–1420. https://doi.org/10.1016/j.cclet.2016.07.011.

(38) Dougherty, T. J.; Gomer, C. J.; Henderson, B. W.; Jori, G.; Kessel, D.; Korbelik, M.; Moan, J.; Peng, Q. Photodynamic Therapy. *JNCI J. Natl. Cancer Inst.* **1998**, *90* (12), 889–905. https://doi.org/10.1093/jnci/90.12.889.

(39) Abrahamse, H.; Hamblin, M. R. New Photosensitizers for Photodynamic Therapy. *Biochem. J.* **2016**, *473* (4), 347–364. https://doi.org/10.1042/BJ20150942.

(40) Josefsen, L. B.; Boyle, R. W. Photodynamic Therapy and the Development of Metal-Based Photosensitisers. *Met.-Based Drugs* **2008**, *2008*, e276109. https://doi.org/10.1155/2008/276109.

(41) Usuda, J.; Kato, H.; Okunaka, T.; Furukawa, K.; Tsutsui, H.; Yamada, K.; Suga, Y.; Honda, H.; Nagatsuka, Y.; Ohira, T.; Tsuboi, M.; Hirano, T. Photodynamic Therapy (PDT) for Lung Cancers. *J. Thorac. Oncol.* **2006**, *1* (5), 489–493. https://doi.org/10.1016/S1556-0864(15)31616-6.

(42) Inoue, K. 5-Aminolevulinic Acid-Mediated Photodynamic Therapy for Bladder Cancer. *Int. J. Urol.* **2017**, *24* (2), 97–101. https://doi.org/10.1111/iju.13291.

(43) O'Connor, A. E.; Gallagher, W. M.; Byrne, A. T. Porphyrin and Nonporphyrin Photosensitizers in Oncology: Preclinical and Clinical Advances in Photodynamic Therapy. *Photochem. Photobiol.* **2009**, *85* (5), 1053–1074. https://doi.org/10.1111/j.1751-1097.2009.00585.x.

(44) Flora Fitzgerald. *Photodynamic Therapy (PDT): Principles, Mechanisms and Applications*; Nova Science Publishers: New York, NY, USA, 2017.

(45) Correia, J. H.; Rodrigues, J. A.; Pimenta, S.; Dong, T.; Yang, Z. Photodynamic Therapy Review: Principles, Photosensitizers, Applications, and Future Directions. *Pharmaceutics* **2021**, *13* (9), 1332. https://doi.org/10.3390/pharmaceutics13091332.

(46) Lee, C.-N.; Hsu, R.; Chen, H.; Wong, T.-W. Daylight Photodynamic Therapy: An Update. *Mol. Basel Switz.* **2020**, *25* (21), E5195. https://doi.org/10.3390/molecules25215195.

(47) Dolmans, D. E. J. G. J.; Fukumura, D.; Jain, R. K. Photodynamic Therapy for Cancer. *Nat. Rev. Cancer* **2003**, *3* (5), 380–387. https://doi.org/10.1038/nrc1071.

(48) Donnelly, R. F.; McCarron, P. A.; Tunney, M. M. Antifungal Photodynamic Therapy. *Microbiol. Res.* **2008**, *163* (1), 1–12. https://doi.org/10.1016/j.micres.2007.08.001.

(49) Rocha, L. G. B. Development of a Novel Photosensitizer for Photodynamic Therapy of Cancer. Ph.D. Thesis, University of Coimbra, Coimbra, Portugal, 2015.

(50) Calixto, G. M. F.; Bernegossi, J.; de Freitas, L. M.; Fontana, C. R.; Chorilli, M. Nanotechnology-Based Drug Delivery Systems for Photodynamic Therapy of Cancer: A Review. *Mol. Basel Switz.* **2016**, *21* (3), 342. https://doi.org/10.3390/molecules21030342.

(51) Agostinis, P.; Berg, K.; Cengel, K. A.; Foster, T. H.; Girotti, A. W.; Gollnick, S. O.; Hahn, S. M.; Hamblin, M. R.; Juzeniene, A.; Kessel, D.; Korbelik, M.; Moan, J.; Mroz, P.; Nowis, D.; Piette, J.; Wilson, B. C.; Golab, J. PHOTODYNAMIC THERAPY OF CANCER: AN UPDATE. *CA. Cancer J. Clin.* **2011**, *61* (4), 250–281. https://doi.org/10.3322/caac.20114.

(52) Lange, N.; Szlasa, W.; Saczko, J.; Chwiłkowska, A. Potential of Cyanine Derived Dyes in Photodynamic Therapy. *Pharmaceutics* **2021**, *13* (6), 818. https://doi.org/10.3390/pharmaceutics13060818.

(53) Ndagi, U.; Mhlongo, N.; Soliman, M. E. Metal Complexes in Cancer Therapy - an Update from Drug Design Perspective. *Drug Des. Devel. Ther.* **2017**, *11*, 599–616. https://doi.org/10.2147/DDDT.S119488.

(54) Zhang, P.; Sadler, P. J. Redox-Active Metal Complexes for Anticancer Therapy. *Eur. J. Inorg. Chem.* **2017**, *2017* (12), 1541–1548. https://doi.org/10.1002/ejic.201600908.

(55) Romero-Canelón, I.; Sadler, P. J. Next-Generation Metal Anticancer Complexes: Multitargeting via Redox Modulation. *Inorg. Chem.* **2013**, *52* (21), 12276–12291. https://doi.org/10.1021/ic400835n.

(56) Abid, M.; Shamsi, F.; Azam, A. Ruthenium Complexes: An Emerging Ground to the Development of Metallopharmaceuticals for Cancer Therapy. *Mini Rev. Med. Chem.* **2016**, *16* (10), 772–786. https://doi.org/10.2174/1389557515666151001142012.

(57) Thota, S. Editorial (Thematic Issue: Anticancer Ruthenium Complexes in Drug Discovery and Medicinal Chemistry). *Mini-Rev. Med. Chem. 16* (10), 771–771.

(58) Southam, H. M.; Butler, J. A.; Chapman, J. A.; Poole, R. K. The Microbiology of Ruthenium Complexes. *Adv. Microb. Physiol.* **2017**, *71*, 1–96. https://doi.org/10.1016/bs.ampbs.2017.03.001.

(59) Aksakal, N. E.; Kazan, H. H.; Eçik, E. T.; Yuksel, F. A Novel Photosensitizer Based on a Ruthenium(II) Phenanthroline Bis(Perylenediimide) Dyad: Synthesis, Generation of Singlet Oxygen and in Vitro Photodynamic Therapy. *New J. Chem.* **2018**, *42* (21), 17538–17545. https://doi.org/10.1039/C8NJ02944J.

(60) Zhou, Q.-X.; Lei, W.-H.; Chen, J.-R.; Li, C.; Hou, Y.-J.; Wang, X.-S.; Zhang, B.-W. A New Heteroleptic Ruthenium(II) Polypyridyl Complex with Long-Wavelength Absorption and High Singlet-Oxygen Quantum Yield. *Chem. – Eur. J.* **2010**, *16* (10), 3157–3165. https://doi.org/10.1002/chem.200902563.

(61) Huang, H.; Yu, B.; Zhang, P.; Huang, J.; Chen, Y.; Gasser, G.; Ji, L.; Chao, H. Highly Charged Ruthenium(II) Polypyridyl Complexes as Lysosome-Localized Photosensitizers for Two-Photon Photodynamic Therapy. *Angew. Chem. Int. Ed.* **2015**, *54* (47), 14049–14052. https://doi.org/10.1002/anie.201507800.

(62) Maia, P. J. S.; de Aguiar, I.; dos Santos Velloso, M.; Zhang, D.; dos Santos, E. R.; de Oliveira, J. R.; Junqueira, J. C.; Selke, M.; Carlos, R. M. Singlet Oxygen Production by a Polypyridine Ruthenium (II) Complex with a Perylene Monoimide Derivative: A Strategy for Photodynamic Inactivation of Candida Albicans. *J. Photochem. Photobiol. Chem.* **2018**, *353*, 536–545. https://doi.org/10.1016/j.jphotochem.2017.12.020.

(63) Juris, A.; Campagna, S.; Balzani, V.; Gremaud, G.; Von Zelewsky, A. Absorption Spectra, Luminescence Properties, and Electrochemical Behavior of Tris-Heteroleptic Ruthenium(II) Polypyridine Complexes. *Inorg. Chem.* **1988**, *27* (20), 3652–3655. https://doi.org/10.1021/ic00293a043.

(64) Juris, A.; Balzani, V.; Barigelletti, F.; Campagna, S.; Belser, P.; von Zelewsky, A. Ru(II) Polypyridine Complexes: Photophysics, Photochemistry, Eletrochemistry, and Chemiluminescence. *Coord. Chem. Rev.* **1988**, *84*, 85–277. https://doi.org/10.1016/0010-8545(88)80032-8.

(65) Balzani, V.; Juris, A. Photochemistry and Photophysics of Ru(II)Polypyridine Complexes in the Bologna Group. From Early Studies to Recent Developments. **2001**. https://doi.org/10.1016/S0010-8545(00)00274-5.

(66) Vögtle, F.; Plevoets, M.; Nieger, M.; Azzellini, G. C.; Credi, A.; De Cola, L.; De Marchis, V.; Venturi, M.; Balzani, V. Dendrimers with a Photoactive and Redox-Active [Ru(Bpy)3]2+-Type Core: Photophysical Properties, Electrochemical Behavior, and Excited-State Electron-Transfer Reactions. *J. Am. Chem. Soc.* **1999**, *121* (26), 6290–6298. https://doi.org/10.1021/ja990430t.

(67) Suzuki, K.; Kobayashi, A.; Kaneko, S.; Takehira, K.; Yoshihara, T.; Ishida, H.; Shiina, Y.; Oishi, S.; Tobita, S. Reevaluation of Absolute Luminescence Quantum Yields of Standard Solutions Using a Spectrometer with an Integrating Sphere and a Back-Thinned CCD Detector. *Phys. Chem. Chem. Phys.* **2009**, *11* (42), 9850–9860. https://doi.org/10.1039/B912178A.

(68) DeRosa, M. C.; Crutchley, R. J. Photosensitized Singlet Oxygen and Its Applications. *Coord. Chem. Rev.* **2002**, *233–234*, 351–371. https://doi.org/10.1016/S0010-8545(02)00034-6.

(69) Friedman, A. E.; Chambron, J. C.; Sauvage, J. P.; Turro, N. J.; Barton, J. K. A Molecular Light Switch for DNA: Ru(Bpy)2(Dppz)2+. *J. Am. Chem. Soc.* **1990**, *112* (12), 4960–4962. https://doi.org/10.1021/ja00168a052.

(70) Wachter, E.; Heidary, D. K.; Howerton, B. S.; Parkin, S.; Glazer, E. C. Light-Activated Ruthenium Complexes Photobind DNA and Are Cytotoxic in the Photodynamic Therapy Window. *Chem. Commun.* **2012**, *48* (77), 9649–9651. https://doi.org/10.1039/C2CC33359G.

(71) Howerton, B. S.; Heidary, D. K.; Glazer, E. C. Strained Ruthenium Complexes Are Potent Light-Activated Anticancer Agents. *J. Am. Chem. Soc.* **2012**, *134* (20), 8324–8327. https://doi.org/10.1021/ja3009677.

(72) Ghannam, J.; Sun, Z.; Cundari, T. R.; Zeller, M.; Lugosan, A.; Stanek, C. M.; Lee, W.-T. Intramolecular C–H Functionalization Followed by a [2σ + 2π] Addition via an Intermediate Nickel–Nitridyl Complex. *Inorg. Chem.* **2019**, *58* (11), 7131–7135. https://doi.org/10.1021/acs.inorgchem.9b00168.

(73) Ghannam, J.; Al Assil, T.; Pankratz, T. C.; Lord, R. L.; Zeller, M.; Lee, W.-T. A Series of 4- and 5-Coordinate Ni(II) Complexes: Synthesis, Characterization, Spectroscopic, and DFT Studies. *Inorg. Chem.* **2018**, *57* (14), 8307–8316. https://doi.org/10.1021/acs.inorgchem.8b00958.

(74) Lugosan, A.; Kawamura, A.; Dickie, D. A.; Zeller, M.; Anderson, J. S.; Lee, W.-T. Magnetically Coupled Iron Azide Chains. *Inorganica Chim. Acta* **2021**, *516*, 120150. https://doi.org/10.1016/j.ica.2020.120150.

(75) Lugosan, A.; Todtz, S. R.; Alcázar, A.; Zeller, M.; Devery, J. J.; Lee, W.-T. Synthesis and Characterization of Trigonal Bipyramidal FeIII Complexes and Their Solution Behavior. *Polyhedron* **2021**, *208*, 115384. https://doi.org/10.1016/j.poly.2021.115384.

(76) Lugosan, A.; Cundari, T.; Fleming, K.; Dickie, D. A.; Zeller, M.; Ghannam, J.; Lee, W.-T. Synthesis, Characterization, DFT Calculations, and Reactivity Study of a Nitrido-Bridged Dimeric Vanadium(IV) Complex. *Dalton Trans.* **2020**, *49* (4), 1200–1206. https://doi.org/10.1039/C9DT04544A.

(77) Lin, H.-J.; Lutz, S.; O'Kane, C.; Zeller, M.; Chen, C.-H.; Assil, T. A.; Lee, W.-T. Synthesis and Characterization of an Iron Complex Bearing a Hemilabile NNN-Pincer for Catalytic Hydrosilylation of Organic Carbonyl Compounds. *Dalton Trans.* **2018**, *47* (10), 3243–3247. https://doi.org/10.1039/C7DT04928E.

(78) Nijegorodov, N.; Luhanga, P. V. C.; Nkoma, J. S.; Winkoun, D. P. The Influence of Planarity, Rigidity and Internal Heavy Atom upon Fluorescence Parameters and the Intersystem Crossing Rate Constant in Molecules with the Biphenyl Basis. *Spectrochim. Acta. A. Mol. Biomol. Spectrosc.* **2006**, *64* (1), 1–5. https://doi.org/10.1016/j.saa.2005.06.032.

(79) Johnson, K. R. D.; Kamenz, B. L.; Hayes, P. G. Bis(Pyrazolyl)Carbazole as a Versatile Ligand for Supporting Lutetium Alkyl and Hydride Complexes. *Organometallics* **2014**, *33* (12), 3005–3011. https://doi.org/10.1021/om500226t.

(80) Lugosan, A. Synthesis and Characterization of Redox Non-Innocent Ligand Supported Transition Metal Complexes. *Dissertations* **2021**.

(81) Biner, M.; Buergi, H. B.; Ludi, A.; Roehr, C. Crystal and Molecular Structures of [Ru(Bpy)3](PF6)3 and [Ru(Bpy)3](PF6)2 at 105 K. *J. Am. Chem. Soc.* **1992**, *114* (13), 5197–5203. https://doi.org/10.1021/ja00039a034.

(82) Karges, J.; Heinemann, F.; Jakubaszek, M.; Maschietto, F.; Subecz, C.; Dotou, M.; Vinck, R.; Blacque, O.; Tharaud, M.; Goud, B.; Viñuelas Zahínos, E.; Spingler, B.; Ciofini, I.; Gasser, G. Rationally Designed Long-Wavelength Absorbing Ru(II) Polypyridyl Complexes as Photosensitizers for Photodynamic Therapy. *J. Am. Chem. Soc.* **2020**, *142* (14), 6578–6587. https://doi.org/10.1021/jacs.9b13620.

(83) Huang, W.; Ogawa, T. Spontaneous Resolution of Δ and Λ Enantiomeric Pair of [Ru(Phen)(Bpy)2](PF6)2 (Phen=1,10-Phenanthroline, Bpy=2,2′-Bipyridine) by Conglomerate Crystallization. *Polyhedron* **2006**, *25* (6), 1379–1385. https://doi.org/10.1016/j.poly.2005.09.033.

(84) Dongare, P.; Myron, B. D. B.; Wang, L.; Thompson, D. W.; Meyer, T. J. [Ru(Bpy)3]2+∗ Revisited. Is It Localized or Delocalized? How Does It Decay? *Coord. Chem. Rev.* **2017**, *345*, 86–107. https://doi.org/10.1016/j.ccr.2017.03.009.

(85) Kober, E. M.; Sullivan, B. P.; Dressick, W. J.; Caspar, J. V.; Meyer, T. J. Highly Luminescent Polypyridyl Complexes of Osmium(II). *J. Am. Chem. Soc.* **1980**, *102* (24), 7383–7385. https://doi.org/10.1021/ja00544a048.

(86) Felix, F.; Ferguson, J.; Güdel, H. U.; Ludi, A. Electronic Spectra of M(Bipy)2+3 Complexions (M = Fe, Ru and Os). *Chem. Phys. Lett.* **1979**, *62* (1), 153–157. https://doi.org/10.1016/0009-2614(79)80432-7.

(87) Felix, F.; Ferguson, J.; Guedel, H. U.; Ludi, A. The Electronic Spectrum of Tris(2,2'-Bipyridine)Ruthenium(2+). *J. Am. Chem. Soc.* **1980**, *102* (12), 4096–4102. https://doi.org/10.1021/ja00532a019.

(88) Arenas, Y.; Monro, S.; Shi, G.; Mandel, A.; McFarland, S.; Lilge, L. Photodynamic Inactivation of Staphylococcus Aureus and Methicillin-Resistant Staphylococcus Aureus with Ru(II)-Based Type I/Type II Photosensitizers. *Photodiagnosis Photodyn. Ther.* **2013**, *10* (4), 615–625. https://doi.org/10.1016/j.pdpdt.2013.07.001.

(89) van der Westhuizen, D.; von Eschwege, Karel G., K. G.; Conradie, J. Electrochemical Data of Polypyridine Complexes of Ru(II). *Data Brief* **2019**, *27*, 104759. https://doi.org/10.1016/j.dib.2019.104759.

(90) Loftus, L. M.; Al-Afyouni, K. F.; Turro, C. New RuII Scaffold for Photoinduced Ligand Release with Red Light in the Photodynamic Therapy (PDT) Window. *Chem. – Eur. J.* **2018**, *24* (45), 11550–11553. https://doi.org/10.1002/chem.201802405.

(91) Zeng, F.; Yu, Z. Construction of Highly Active Ruthenium(II) NNN Complex Catalysts Bearing a Pyridyl-Supported Pyrazolyl-Imidazolyl Ligand for Transfer Hydrogenation of Ketones. *Organometallics* **2009**, *28* (6), 1855–1862. https://doi.org/10.1021/om801080p.

(92) Betley, T. A.; Qian, B. A.; Peters, J. C. Group VIII Coordination Chemistry of a Pincer-Type Bis(8-Quinolinyl)Amido Ligand. *Inorg. Chem.* **2008**, *47* (24), 11570–11582. https://doi.org/10.1021/ic801047s.

(93) Avci, P.; Gupta, A.; Sadasivam, M.; Vecchio, D.; Pam, Z.; Pam, N.; Hamblin, M. R. Low-Level Laser (Light) Therapy (LLLT) in Skin: Stimulating, Healing, Restoring. *Semin. Cutan. Med. Surg.* **2013**, *32* (1), 41–52.

(94) Barolet, D. Light-Emitting Diodes (LEDs) in Dermatology. *Semin. Cutan. Med. Surg.* **2008**, *27* (4), 227–238. https://doi.org/10.1016/j.sder.2008.08.003.

(95) Lincoln, R.; Kohler, L.; Monro, S.; Yin, H.; Stephenson, M.; Zong, R.; Chouai, A.; Dorsey, C.; Hennigar, R.; Thummel, R. P.; McFarland, S. A. Exploitation of Long-Lived 3IL Excited States for Metal–Organic Photodynamic Therapy: Verification in a Metastatic Melanoma Model. *J. Am. Chem. Soc.* **2013**, *135* (45), 17161–17175. https://doi.org/10.1021/ja408426z.

(96) van der Sluis, P.; Spek, A. L. BYPASS: An Effective Method for the Refinement of Crystal Structures Containing Disordered Solvent Regions. *Acta Crystallogr. A* **1990**, *46* (3), 194–201. https://doi.org/10.1107/S0108767389011189.

(97) Sheldrick, G. M. Crystal Structure Refinement with SHELXL. *Acta Crystallogr. Sect. C Struct. Chem.* **2015**, *71* (1), 3–8. https://doi.org/10.1107/S2053229614024218.

(98) Hübschle, C. B.; Sheldrick, G. M.; Dittrich, B. ShelXle: A Qt Graphical User Interface for SHELXL. *J. Appl. Crystallogr.* **2011**, *44* (6), 1281–1284. https://doi.org/10.1107/S0021889811043202.

(99) Sheldrick, George M. **2018**.

(100) APEX3 V2019.1, Bruker AXS Inc., Madison, WI, USA, **2019**.

(101) SAINT V8.40B, Bruker AXS Inc., Madison, WI, USA, **2016**.

VITA

Keit Dine was born in Vlore, Albania, in September of 1997 before moving to Elmwood Park, IL, where he spent his formative years. He attended Loyola University Chicago where in 2020 he received a Bachelor of Science in Biochemistry. While at Loyola he worked under the guidance of Dr. Wei-Tsung Lee and studied the synthesis and characterization of transition-metal complexes.

Dine stayed at Loyola University Chicago for his graduate studies to peruse a Master of Science in Chemistry. He continued to work under the supervision of Dr. Wei-Tsung Lee and focused on ruthenium complexes. After the completion of his degree, he will be preparing to apply to medical school.